Advanced Virgo Calibration Monitoring during the Observing Run O3

D. Verkindt, L. Rolland, D. Estevez, B. Mours, P. Lagabbe, M. Seglar-Arroyo

May 28, 2021

VIR-0544A-21
https://tds.virgo-gw.eu/ql/?c=16792

Contents

1 Introduction

Over all the O3 run, from April 1st 2019 to March 27th 2020, a permanent monitoring has been performed on the modulus and phase of the reconstructed gravitational wave strain $h(t)$ or on the phase and modulus of transfer functions of various signals used for the calibration of the Advanced Virgo detector [1].

Such monitoring has been done by injecting sinusoidal excitations (calibration lines) through the Photon Calibrator (PCal) [2][4][3] or through the Electromagnetic (EM) actuators that control the interferometer's mirrors longitudinal motion. Part of this monitoring was done by the online running process TFMoni [5] and provided useful information about the accuracy of the EM actuators response and useful checks of the $h(t)$ reconstruction uncertainties.

This note summarizes the main results obtained and provides details about the computations and procedures that allowed to get those results.

Most of the systematic uncertainties on $h(t)$ phase and modulus have been obtained by looking at the variation in time of the calibration parameters or, more globally, the variation in time of the reconstructed $h(t)$ with respect to a modeled value h_{inj}.

Such variations were correlated to changes of the interferometer working point during the O3 time period. Figure 1 shows the time evolution of the BNS range over the O3 observation run and illustrates the time scale and amplitude of those changes.

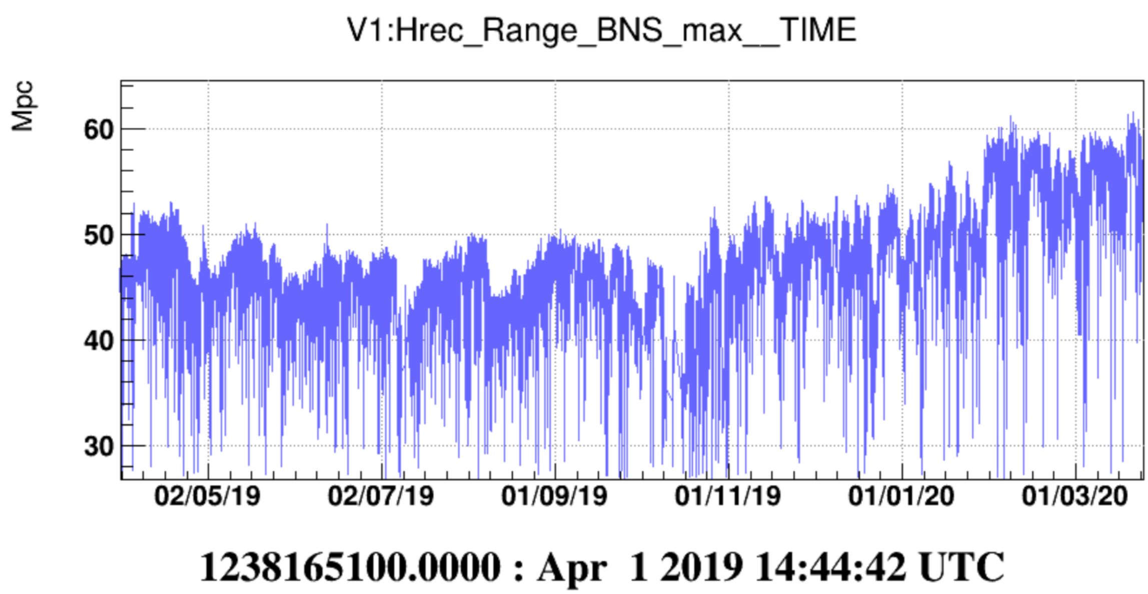

Figure 1: Evolution of the BNS range over the O3 time period.

2 Permanent calibration lines injected during O3

During O3, permanent lines (sine wave signals) were injected continuously on the WE, NE, PR and BS mirrors and marionette electromagnetic actuators and on the WE and NE mirrors Photon Calibrators (PCal). The table 1 gives the full list of those permanent lines.
Two paths for injections have been used:

1. **CORR**: calibration signal is added to the control signal (Z_CORR on the EM actuators). This type of injection can be done on all mirrors and marionettes, and the calibration lines are naturally subtracted in the $h(t)$ reconstruction process, along with the control signal: hence they are already subtracted at the level of the h_{raw} signal.

2. **HI**: calibration signal is added as hardware injection on NE and WE (Z_NOISE on EM actuators or photon calibrators). Such injections are done via NE and WE mirrors and are not subtracted in the first step of the $h(t)$ reconstruction. They are specifically subtracted as hardware injections (HI) in the last step of the reconstruction (after the noise subtraction) when going from h_{clean} to the final $h(t)$ signal.

The $h(t)$ reconstruction process requires four lines sent to the four mirrors EM actuators (BS, PR, NE, WE) to monitor the optical gain and arm cavity finesse (see section 4). Those four lines are part of the CORR lines.

Both CORR and HI injections can be used to monitor the actuator responses (see section 6). In addition, the HI injections have been used to monitor the $h(t)$ reconstruction (see section 7) and to estimate the O3 $h(t)$ uncertainties.

The lines at 2012.5 Hz sent onto all the mirror's and marionette's actuators were well below the Virgo sensitivity. However, since the control signals are very low at this frequency, they were strong enough to be seen in the correction signal sent back by the actuator DSP. Thus, the transfer functions between the correction signal Sc_MIR_Z_CORR and the injected signal CAL_MIR_Z_CORR have been used to monitor the data transfer from the real-time PC to the DSPs and to highlight any change in the DSP digital processing.

Type	Frequency (Hz)	Mirror	Actuator
CORR	15.8	WE mar.	EM
	16.3	BS mar.	EM
	16.8	NE mar.	EM
	61.0	BS mir.	EM
	61.5	WE mir.	EM
	62.5	NE mir.	EM
	63.0	PR mir.	EM
	353.0	PR mir.	EM
	356.0	BS mir.	EM
	356.5	WE mir.	EM
	357.5	NE mir.	EM
	2012.5	PR, BS, NE, WE mir	EM
	2012.5	NI, WI mir	EM
	2012.5	BS, NE, WE mar	EM
HI	34.5	NE mir.	PCal
	36.5	WE mir.	PCal
	37.5	NE mir.	EM
	56.5	WE mir.	EM
	60.5	WE mir.	PCal
	63.5	NE mir.	PCal
	77.5	NE mir.	EM
	106.5	WE mir.	EM
	107.5	NE mir.	EM
	136.5	NE mir.	EM
	206.5	WE mir.	EM
	406.5	WE mir.	EM

Table 1: List of all permanent calibration lines injected during O3 through the mirror and marionetta EM actuators or through the Pcal actuators.

3 The TFMoni monitoring process

An online process, named TFMoni, has been used during all the O3 run to compute various Transfer Functions (TF) in order to monitor the electromagnetic actuators, the photon calibrator and the $h(t)$ reconstruction.

TFMoni computed all the TF values with an average of 12 FFTs (or 24 FFTs in case of PCal), each FFT being computed over 10 s of data, with an overlap of 50%. It used a moving averaging, thus for a given TF, one output value was computed every 5 s. The TFMoni output channels were sampled at 1 Hz and thus contained five times the same value every 5 s.

TFMoni uses the library Frv which has a convention in the binning of the FFTs. The version of TFMoni that ran online during O3 was not aligned with this convention and the bin chosen in the FFT for a given frequency was not the correct one. As a result, the TF was computed one bin lower, a bin where the line signal is still present but reduced in amplitude by a factor $\sqrt{2}$ in the FFTs. The estimated TF modulus and phase being ratio and difference of two FFTs, the measured values were correct, but the associated uncertainties were higher than expected by a factor $\sqrt{2}$. We have thus reprocessed the TFs used for monitoring the reconstructed $h(t)$ bias (section 7) over all O3b (using data on Virgo site) and over all O3a (using data at CCin2p3) to provide the correct TFMoni values used to get the results shown in this note and in the O3 calibration paper. Note that we did not reprocess the TFs used for coil monitoring (section 6), so the width of the distributions shown for these are overestimated by a factor $\sqrt{2}$.

In addition to this problem of FFT binning, the configuration used online during O3 had wrong frequencies for the monitoring of the TF between BS (PR) coil voltages and BS (PR) control signals. No reprocessing has been done to fix this problem. Just be aware that in the cases of BS and PR actuators, the TFMoni results for the coil voltages (VOUT signals) monitoring are not provided at the frequencies where the permanent lines were injected.

The TFMoni configuration used online during O3 is available in the appendix A. Figure 2 shows an example of input signals used in this configuration.

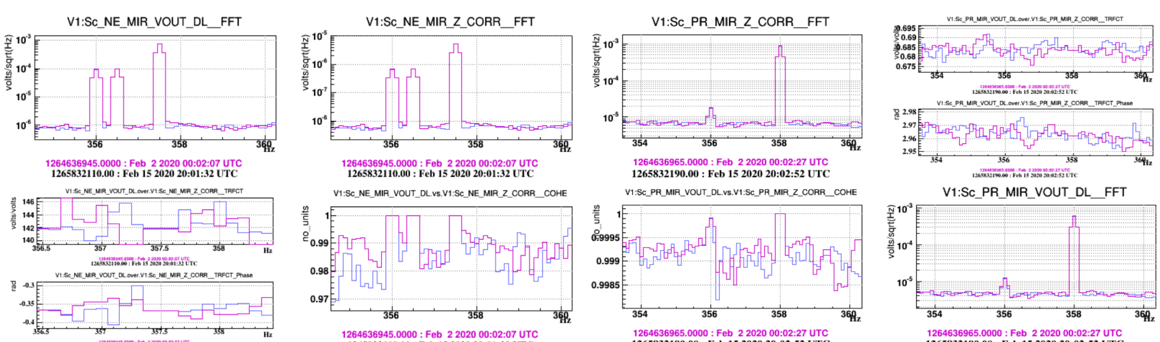

Figure 2: Examples of signals used by TFMoni. Left is for NE mirror, right is for PR mirror. Each time, the FFT of the signals, their coherence and their transfer function are shown, for two dates of O3b. We can see the injected lines used by TFMoni at 357.5 HZ (for NE) and 358 Hz (for PR).

4 Calibration lines for optical gain and finesse monitoring

Four lines were injected on WE, NE, PR and BS mirrors around 60 Hz, through the control signals via electromagnetic actuators. They were used in the $h(t)$ reconstruction process to monitor the optical gains and finesse of each arm's cavity. The lines were injected permanently and this monitoring was done at the pace of $h(t)$ reconstruction, that is once every 4 s.

The lines were injected at well defined frequencies and with a Signal-to-Noise Ratio (SNR) of the order of 100 above the background noise, as summarized in the table 2 (see section 8 for details about the SNR computation). They were naturally subtracted in the $h(t)$ reconstruction algorithm since they were present in the longitudinal control signals. Figure 3 shows those calibration lines in the spectrum of the dark fringe signal and in the spectrum of the reconstructed $h(t)$.

Injection source	Line frequency	Line SNR
NE mirror actuator	62.5 Hz	117
WE mirror actuator	61.5 Hz	103
BS mirror actuator	61.0 Hz	125
PR mirror actuator	63.0 Hz	3

Table 2: Permanent calibration lines injected during O3 through the EM actuators to monitor the optical gain and finesse of the arm cavities in the h(t) reconstruction processing. The given SNR has been estimated in the Hrec_hoft_raw_20000Hz channel (i.e. before noise subtraction) for GPS=1264636818 (O3b).

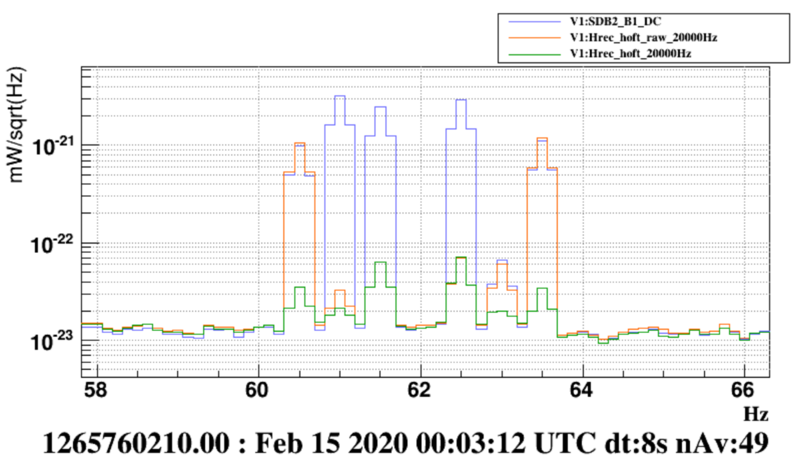

Figure 3: Calibration lines in the spectrum of h(t), before h reconstruction (blue, B1 spectrum normalized to match h spectrum around 60 Hz), after h reconstruction (orange) and in the final h(t) delivered to data analyses (green) with calibration lines subtracted.

5 Monitoring with Photon Calibrator lines

In addition, a set of permanent lines were injected on NE and WE as hardware injections (HI lines of table 1) via the EM and Pcal actuators, at various frequencies and SNRs. They were used to monitor the PCal and the EM actuators as well as the $h(t)$ reconstruction stability (see tables 6 and 7 of section 7). These hardware injections were subtracted in the last step of the $h(t)$ reconstruction process. An example is seen in figure 3, where the two hardware injections sent via the PCal at 60.5 Hz and 63.5 Hz are subtracted in the final $h(t)$ channel (green curve).

Among those lines, four lines were injected at the Photon Calibrator level, with a high SNR of about 40 around 60 Hz in O3b. They are listed in the table 3 and their subtraction in the $h(t)$ reconstruction process is illustrated by the Figure 4.

Injection source	Line frequency	Line SNR
NE PCal	34.5 Hz	12
WE PCal	36.5 Hz	14
NE PCal	60.5 Hz	47
WE PCal	63.5 Hz	41

Table 3: Permanent calibration lines injected during O3 through the Photon Calibrator to monitor the $h(t)$ reconstruction process. The given SNR has been estimated in the Hrec_hoft_raw_20000Hz channel (i.e. before noise subtraction) for GPS=1264636818 (O3b). Lower values were obtained for O3a.

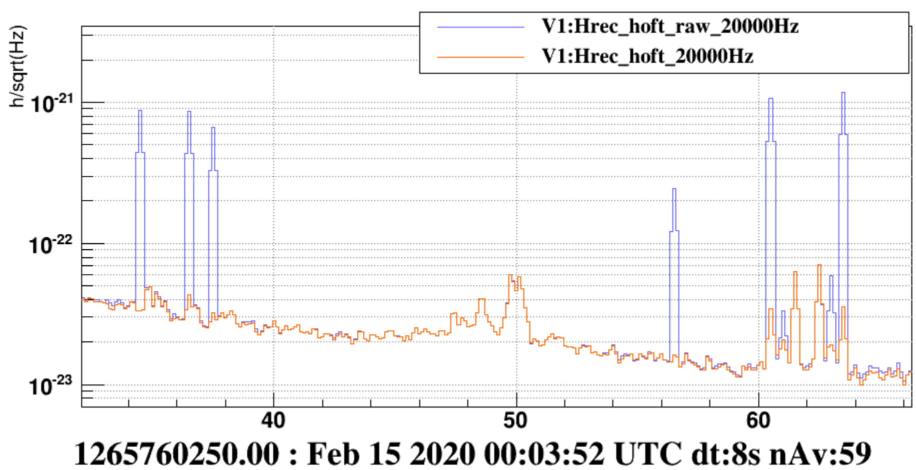

Figure 4: PCal calibration lines in the spectrum of Hrec_hoft_raw_20000Hz (blue) and in the spectrum of Hrec_hoft_20000Hz (orange), which is the final $h(t)$ delivered to data analyses, with the four PCal calibration lines (and other) subtracted.

6 Monitoring of the EM actuators coils

In order to monitor the EM longitudinal actuator responses (NE, WE, BS and PR), the transfer functions from the correction signals to the current flowing in the actuator coils have been computed and monitored (i.e. transfer functions like Sc_NE_MIR_VOUTDL / Sc_NE_MIR_Z_CORR). Such monitoring include the analog part of the actuators.

The computation was done online with the TFMoni process described briefly in section 3. The transfer functions were computed at frequencies around 60 Hz and 355 Hz.

The fluctuations of the transfer function modulus and phase, at a given frequency, between each of these coil voltages and the corresponding longitudinal control loop signal allowed to estimate the stability of the EM actuators response used for the h(t) reconstruction. As an example, the modulus and phase of those transfer functions for NE and WE VOUTDL coils (VOUTDL is for Voltage in Down Left coil) are shown on figure 5. The full set of plots is available in appendix A and full results for NE, WE, BS and PR coils, around 60 Hz and around 355 Hz, are shown in tables 4 and 5.

The plots show variations that are quite stable all along the run, despite the fact that between O3a and O3b the SNR of the injected lines has changed a lot in the control loop signals as can be seen in table 4 and figure 6. This is a hint that the uncertainty on the TF is limited by the VOUT signals and not by the control signals.

The variation of the SNR between O3a and O3b in tables 4 and 5 is mainly due to a reduction of the noise in the control loop correction signals Sc_XX_MIR_Z_CORR (XX=BS,PR,NE or WE) at the frequencies where are estimated the lines SNR. This is illustrated by the plots of Figure 6.

In general, the distributions of the modulus and phase over O3a and O3b are Gaussian with statistical errors of the order of 0.4% in modulus and 3 mrad in phase. Except for NE and WE around 355 Hz (see for example figures 24 and 32) where the statistical errors are much lower and the distribution not Gaussian. Indeed, the SNR being ten times higher at these frequencies, some systematic time variations are clearly highlighted, at the level of 0.04% in modulus and 0.1 mrad in phase (see figures and table 4).

Overall, except some modifications done during the run and described within the caption of the figures, **the observed variations of the TF between VOUT signals and control loop signals are within around 0.5% in modulus and 3 mrad in phase, mainly limited by statistical errors**.

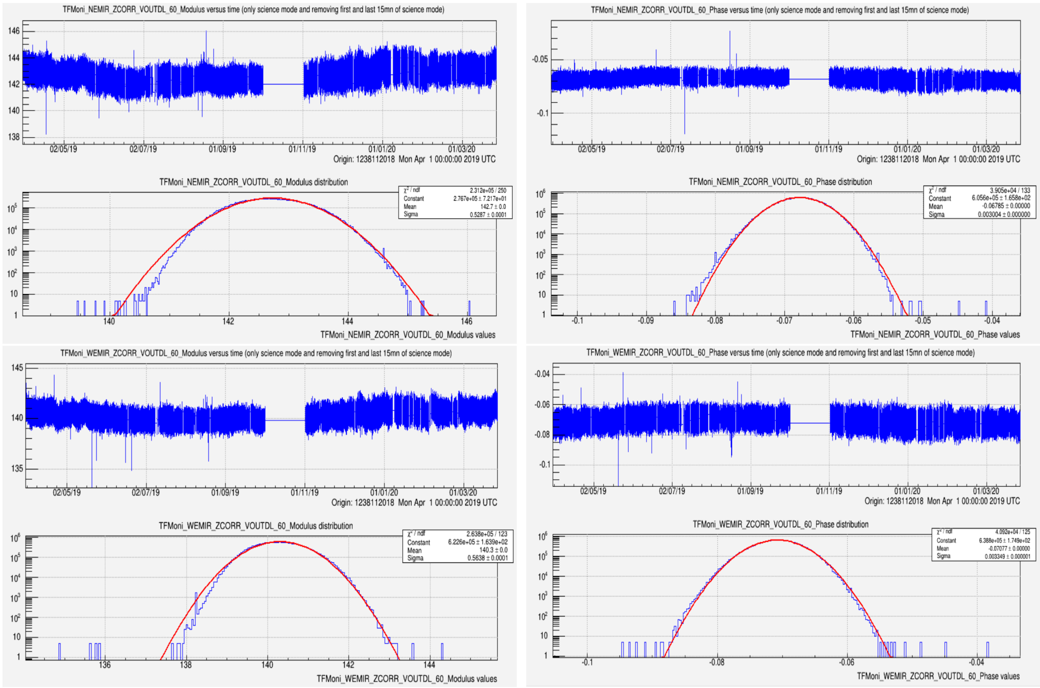

Figure 5: TFMoni Modulus and Phase near 60 Hz of the transfer function between NE (WE) coil voltages VOUT_DL and the longitudinal control loop signals Sc_NE_MIR_Z_CORR (Sc_WE_MIR_Z_CORR) . For each plot, time evolution and fitted distribution are shown. Plots for all actuators and all frequencies are available in appendix A.

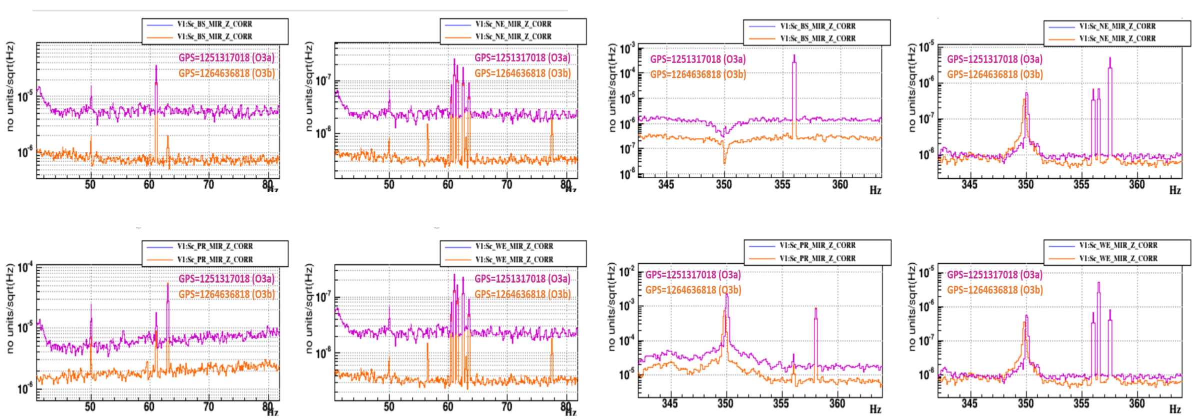

Figure 6: O3a and O3b superposed spectra of the longitudinal control loop signals Sc_XX_MIR_Z_CORR (XX=BS,PR,NE and WE) around 60 Hz (left) and around 355 Hz (right).

Actuator Coil	Line freq.	O3a SNR	O3b SNR	σ_{mod}	σ_{phi}
NE VOUTUL_60	62.5 Hz	3	20	0.37%	2.8 mrad
NE VOUTUR_60	62.5 Hz	3	20	0.39%	3.1 mrad
NE VOUTDL_60	62.5 Hz	3	20	0.36%	3.0 mrad
NE VOUTDR_60	62.5 Hz	3	20	0.37%	3.0 mrad
NE VOUTUL_355	357.5 Hz	220	260	0.034%	0.09 mrad
NE VOUTUR_355	357.5 Hz	220	260	0.036%	0.08 mrad
NE VOUTDL_355	357.5 Hz	220	260	0.027%	0.06 mrad
NE VOUTDR_355	357.5 Hz	220	260	0.035%	0.08 mrad
WE VOUTUL_60	61.5 Hz	3	18	0.37%	3.2 mrad
WE VOUTUR_60	61.5 Hz	3	18	0.40%	3.5 mrad
WE VOUTDL_60	61.5 Hz	3	18	0.40%	3.3 mrad
WE VOUTDR_60	61.5 Hz	3	18	0.43%	3.7 mrad
WE VOUTUL_355	356.5 Hz	260	340	0.028%	0.06 mrad
WE VOUTUR_355	356.5 Hz	260	340	0.037%	0.05 mrad
WE VOUTDL_355	356.5 Hz	260	340	0.060%	0.17 mrad
WE VOUTDR_355	356.5 Hz	260	340	0.027%	0.06 mrad

Table 4: The SNR of the lines used to monitor the modulus and phase of the transfer functions between the longitudinal control loop signals and XX coil voltages (XX=NE,WE), around 60 Hz and around 355 Hz, have been estimated at GPS=1251317018 (O3a) and GPS=1264636818 (O3b), in the Sc_XX_MIR_Z_CORR channel. Are shown also the statistical fluctuations over the full O3 run taken as the width provided by a Gaussian fit of the distribution of the module or phase values. Such TFMoni values were not reprocessed (unlike in section 7) and the uncertainties on modulus and phase are thus a factor $\sqrt{2}$ larger than what they should be.

Actuator Coil	Line freq.	O3a SNR	O3b SNR	σ_{mod}	σ_{phi}
BS VOUTUL_60	62.8 Hz	3	17	0.18%	1.9 mrad
BS VOUTUR_60	62.8 Hz	3	17	0.19%	4.3 mrad
BS VOUTDL_60	62.8 Hz	3	17	0.19%	1.8 mrad
BS VOUTDR_60	62.8 Hz	3	17	0.19%	4.3 mrad
BS VOUTUL_355	357.8 Hz	147	750	0.53%	5.3 mrad
BS VOUTUR_355	357.8 Hz	147	750	0.35%	9.0 mrad
BS VOUTDL_355	357.8 Hz	147	750	0.42%	4.8 mrad
BS VOUTDR_355	357.8 Hz	147	750	0.49%	10.2 mrad
PR VOUTUL_60	62.3 Hz	3	11	1.03%	10.4 mrad
PR VOUTUR_60	62.3 Hz	3	11	0.98%	9.8 mrad
PR VOUTDL_60	62.3 Hz	3	11	1.13%	11.0 mrad
PR VOUTDR_60	62.3 Hz	3	11	1.03%	10.3 mrad
PR VOUTUL_355	357.3 Hz	18	52	0.23%	2.2 mrad
PR VOUTUR_355	357.3 Hz	18	52	0.20%	2.0 mrad
PR VOUTDL_355	357.3 Hz	18	52	0.26%	2.5 mrad
PR VOUTDR_355	357.3 Hz	18	52	0.24%	2.3 mrad

Table 5: The SNR of the lines used to monitor the modulus and phase of the transfer functions between the longitudinal control loop signals and XX coil voltages (XX=BS,PR), around 60 Hz and around 355 Hz, have been estimated at GPS=1251317018 (O3a) and GPS=1264636818 (O3b), in the Sc_XX_MIR_Z_CORR channel. Are shown also the statistical fluctuations over the full O3 run taken as the width provided by a Gaussian fit of the distribution of the module or phase values. CAUTION: BS and PR measurements were done by TFMoni at frequencies where injected lines were not present (62.8 Hz instead of 61 Hz, 357.8 Hz instead of 356 Hz, 62.3 HZ instead of 63 Hz, and 357.3 Hz instead of 358 Hz), so the numbers for BS and PR are not at the frequencies of the injected lines. Such TFMoni values were not reprocessed (unlike in section 7) and the uncertainties on modulus and phase are thus a factor $\sqrt{2}$ larger than what they should be.

7 Monitoring of the reconstructed h(t) channel bias via hardware injections

The set of twelve permanent sinusoidal signals, listed in tables 6 and 7, were injected during O3 on the end mirrors via the different PCal and electromagnetic actuators. They allow a continuous comparison of the reconstructed strain data h_{rec} with the injected equivalent strain h_{inj} in the most sensitive band of the detector, between 35 Hz and 400 Hz. Some signals are in the regions where the bias of the strain channel is the highest, i.e. 100 to 200 Hz for the amplitude and 60 to 90 Hz for the phase. Hence they have been used to monitor possible time variations of this bias.

The modulus and phase of the h_{rec}/h_{inj} transfer functions at the twelve injected frequencies were computed online using a moving average of 12 (24 for the PCal) 10 s-long FFTs and provided in the online data stream as channels sampled at 1 Hz. The h_{inj} signals were estimated with online models set at the beginning of O3 and they were not updated in this processing during O3. As such, the monitoring of these channels is a witness of the possible variations of the reconstructed strain data, as well as of the small variations of the actuator responses as described earlier, but they are not precise witness of the absolute value of the strain data bias.

The distributions of the online modulus and phase have been built over O3a and O3b and are shown in the plots of appendix A. Their standard deviations are reported in tables 6 and 7. For every injected signal, the typical SNR during O3a and O3b is also given, as well as the expected standard deviation of the modulus in case of statistical fluctuations only. The measured variations during O3a and O3b (Fig. 7) are all slightly larger than the expected statistical fluctuations only: it indicates that these monitoring channels indeed highlight time variations of the h_{rec}/h_{inj} ratio. These variations can be considered as systematic uncertainty and are estimated by subtracting quadratically the expected statistical fluctuations from the measured one. They are shown, for O3a and O3b, in the two plots of figure 8.

For O3a and O3b, the h_{rec}/h_{inj} modulus systematic uncertainty is estimated to be of 0.9%, at 137.5 Hz, while the phase systematic uncertainty is estimated to be of 9 mrad. These variations include both $h(t)$ bias variations and variations of the actuator responses. They have been used as conservative estimate of the uncertainty on $h(t)$ bias.

Actuator	Line freq.	Line SNR	σ_{stat}	O3a σ_{mod}	O3a σ_{phi}
NE EM	37.5 Hz	3	1.06%	1.57%	15.8 mrad
NE EM	77.5 Hz	4.5	0.70%	1.58%	15.5 mrad
NE EM	107.5 Hz	13	0.25%	0.60%	6.8 mrad
NE EM	137.5 Hz	7.5	0.43%	1.00%	10.1 mrad
NE PCal	34.5 Hz	6	0.37%	0.95%	9.1 mrad
NE PCal	63.5 Hz	25	0.09%	0.32%	2.3 mrad
WE EM	56.5 Hz	5	0.66%	1.40%	13.9 mrad
WE EM	106.5 Hz	11	0.29%	0.71%	7.3 mrad
WE EM	206.5 Hz	11	0.29%	0.71%	6.2 mrad
WE EM	406.5 Hz	9.5	0.34%	0.79%	7.6 mrad
WE PCal	36.5 Hz	5	0.44%	0.90%	8.4 mrad
WE PCal	60.5 Hz	22	0.10%	0.35%	2.5 mrad

Table 6: Sinusoidal permanent hardware injections used during O3a to monitor the accuracy of $h(t)$ reconstruction. For the four different end test mass actuators, the injected line frequency is given with the typical signal-to-noise ratio estimated during O3a, the expected standard deviation of the h_{rec}/h_{inj} modulus in case of statistical fluctuations only, and the standard deviations measured on the TFMoni distributions of the modulus and phase of h_{rec}/h_{inj} during O3a.

Actuator	Line freq.	Line SNR	σ_{stat}	O3b σ_{mod}	O3b σ_{phi}
NE EM	37.5 Hz	11	0.29%	0.77%	8.9 mrad
NE EM	77.5 Hz	7	0.46%	1.20%	12.0 mrad
NE EM	107.5 Hz	16	0.20%	0.55%	6.4 mrad
NE EM	137.5 Hz	9	0.36%	0.91%	10.0 mrad
NE PCal	34.5 Hz	12	0.18%	0.53%	5.5 mrad
NE PCal	63.5 Hz	41	0.06%	0.34%	1.8 mrad
WE EM	56.5 Hz	7	0.46%	1.05%	10.6 mrad
WE EM	106.5 Hz	14	0.23%	0.62%	7.1 mrad
WE EM	206.5 Hz	15	0.22%	0.73%	5.8 mrad
WE EM	406.5 Hz	12	0.27%	0.77%	7.4 mrad
WE PCal	36.5 Hz	14	0.16%	0.54%	6.7 mrad
WE PCal	60.5 Hz	47	0.04%	0.34%	2.0 mrad

Table 7: Sinusoidal permanent hardware injections used during O3b to monitor the accuracy of $h(t)$ reconstruction. For the four different end test mass actuators, the injected line frequency is given with the typical signal-to-noise ratio estimated during O3b, the expected standard deviation of the h_{rec}/h_{inj} modulus in case of statistical fluctuations only, and the standard deviations measured on the TFMoni distributions of the modulus and phase of h_{rec}/h_{inj} during O3b.

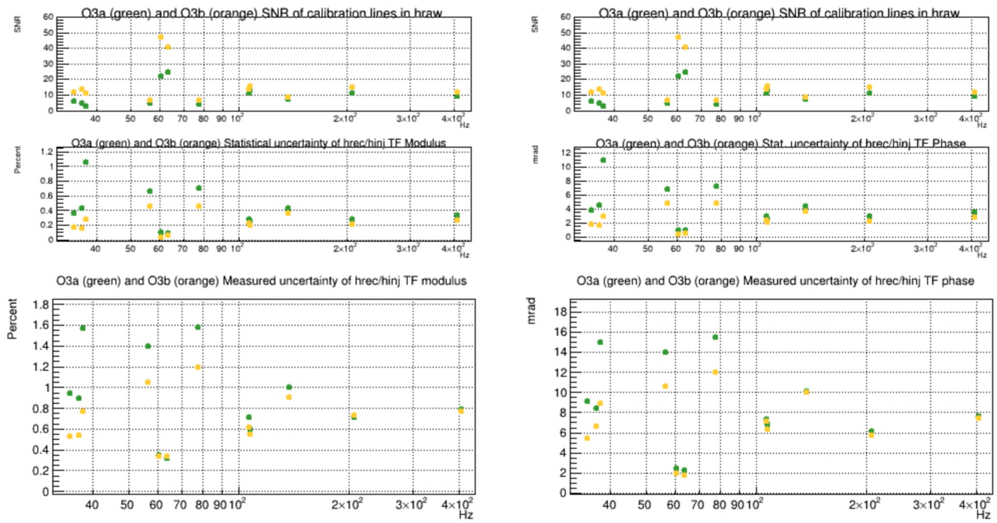

Figure 7: Upper left: SNR of the permanent injected lines used for hrec/hinj monitoring and the statistical uncertainties on modulus deduced from SNR (SNR were estimated at GPS=1251525400 for O3a and GPS=1265000000 for O3b). Upper right: same for the statistical uncertainties on phase of hrec/hinj. Lower left: widths of the hrec/hinj modulus distributions obtained from TFMoni. Lower right: widths of the hrec/hinj phase distributions obtained from TFMoni.

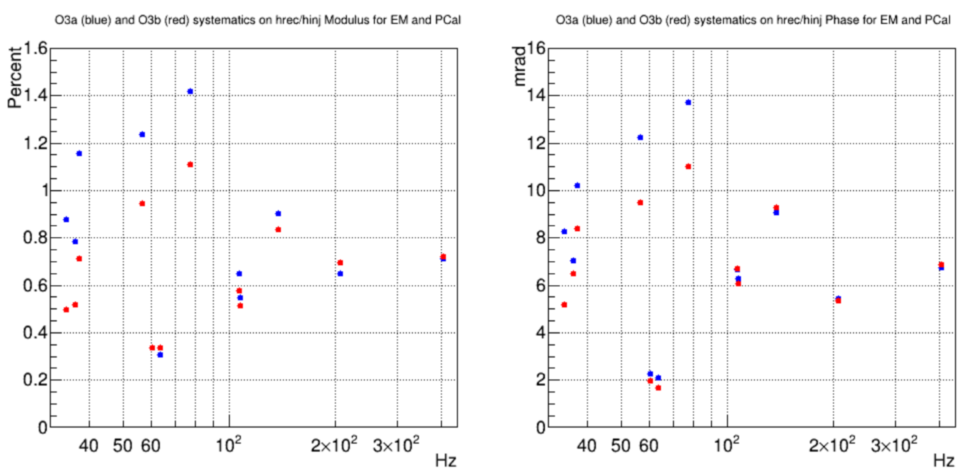

Figure 8: Left: systematic uncertainties on hrec/hinj module computed as the quadratic difference between the measured width and the expected statistical uncertainties (blue for O3a and red for O3b). Statistical uncertainties have been estimated using a SNR computed at GPS=1251525400 for O3a and GPS=1265000000 for O3b. Right: systematic uncertainties on hrec/hinj phase computed as the quadratic difference between the measured width and the computed statistical uncertainties (blue for O3a and red for O3b). Details about statistical uncertainties estimation are provided in section 8.

8 Details about the SNR and statistical uncertainty computations

The SNR of the injected lines is estimated using the calisnr.C ROOT script of the CaliSimu package. This script uses 3 bins of the spectrum around the line frequency and uses the following formula:

$$SNR^2 = \frac{s_{i-1}^2 + s_i^2 + s_{i+1}^2}{b_{i-1}^2 + b_i^2 + b_{i+1}^2} \times \frac{1}{T} = \frac{(1 + 1/4 + 1/4) \times s_i^2}{3 \times b_i^2} \times \frac{1}{T} = 0.5 \times \frac{s_i^2}{b_i^2} \times \frac{1}{T}$$

where T is the duration of the FFT, s_i is the FFT amplitude at the frequency of the injected line (that is the rms of the sinusoidal excitation signal), b_i is the estimated noise level at the frequency of the injected line. Finally, the SNR of the injected line is:

$$SNR = \frac{1}{\sqrt{2}} \times \frac{s_i}{b_i} \times \sqrt{\frac{1}{T}}$$

Then, the estimation of the relative statistical uncertainty $\sigma_{modulus}$ on the modulus is done by considering that the injected line is within a stationary Gaussian noise whose spectrum has, in each frequency bin, a Gaussian random variable whose rms value is 0.5 time its mean value (which is the level of the amplitude spectral density).

$$\sigma = 0.5 \times b(i) \times \sqrt{\frac{1}{N_{fft}}}$$

where N_{fft} is the number of averaged FFTs. Then, by replacing b_i by its expression with s_i and SNR, we get the relative statistical uncertainty:

$$\sigma_{modulus} = \frac{\sigma}{s_i} = 0.5 \times \frac{1}{\sqrt{2}} \times \frac{1}{SNR} \times \sqrt{\frac{1}{N_{fft}}}$$

The values of $\sigma_{modulus}$ estimations are provided in tables 6, 7 or 4.

The statistical uncertainty on the phase in mrad is computed on the basis of the following formula, deduced from the uncertainties on TF modulus and phase based on the coherence value in [10].

$$\sigma_{phase}(mrad) = 10 \times 0.88/0.85 \times \sigma_{modulus}$$

The computation of $\sigma_{modulus}$ is done using an estimation of the SNR at a given time. Figure 9 shows an example of the time evolution of the SNR over the run O3, for four calibration lines in the channel Hrec_hoft_raw_20000Hz. Except some drops due to the presence of glitches, the SNR value fluctuations are below 20%, thus all the statistical uncertainties deduced from the SNR value does not fluctuates more than 20% over the O3 run.

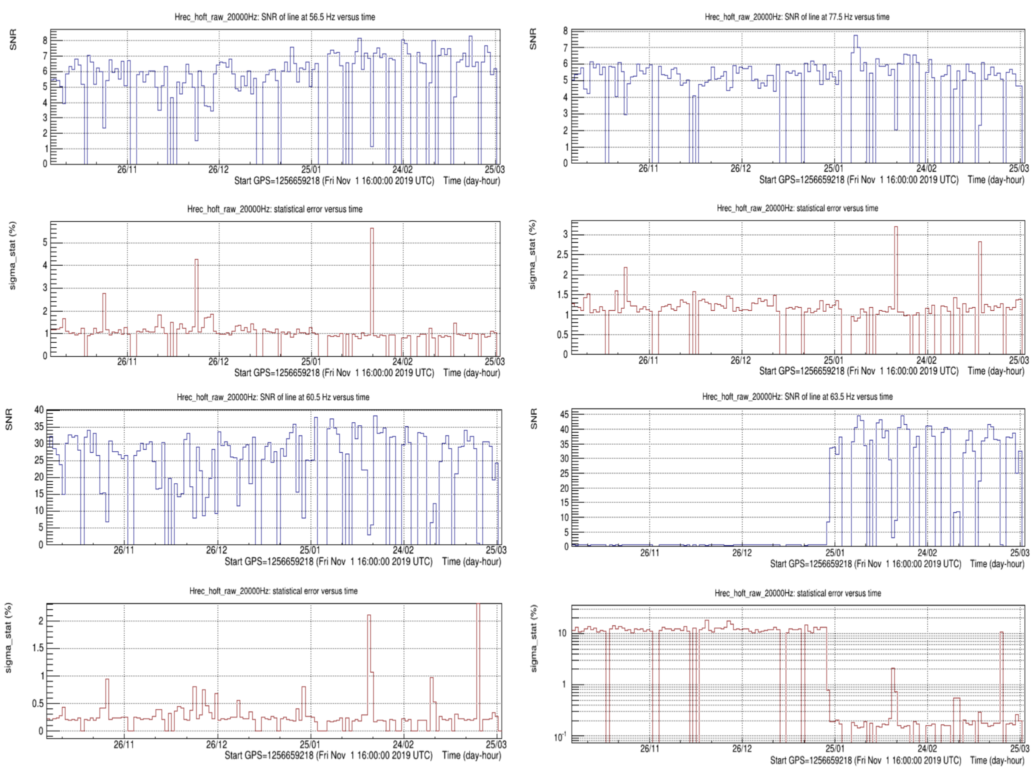

Figure 9: Time evolution over the O3b run of the SNR of calibration lines (and corresponding statistical uncertainty) at 56.5 Hz (upper left), 77.5 Hz (upper right), 60.5 Hz (lower left) and 63.5 Hz (lower right ; warning: this line was injected via the NE Pcal, which was not working between October 2019 and end January 2020, this explains the close to zero SNR of the line in this time period).

References

[1] F Acernese et al., Advanced Virgo: a second-generation interferometric gravitational wave detector. Classical Quantum Grav. **32**, (2):024001 (2015)

[2] Estevez et al., The Advanced Virgo Photon Calibrators, Classical Quantum Grav. **38**, (1):075007 (2021) , arXiv:2009.08103

[3] Virgo note VIR-0013A-15, https://tds.virgo-gw.eu/ql/?c=10722

[4] Virgo note VIR-0466A-19, https://tds.virgo-gw.eu/ql/?c=14294

[5] TFMoni Documentation, Virgo note VIR-0459A-21, https://tds.virgo-gw.eu/ql/?c=16707

[6] The Frame Vector library (Frv): https://lappweb.in2p3.fr/virgo/FrameL/, https://git.ligo.org/virgo/virgoapp/Frv

[7] CaliSimu documentation, Virgo note VIR-0037B-21, https://tds.virgo-gw.eu/ql/?c=16285

[8] F. Acernese et al., Calibration of Advanced Virgo and Reconstruction of the Gravitational Wave Signal h(t) during the Science Run O2 , Classical and Quantum Gravity, vol.35 no 20 (2018) , arXiv:1807.03275

[9] Hrec package documentation, Virgo note VIR-0590A-20 , https://tds.virgo-gw.eu/ql/?c=17373

[10] Calibration and sensitivity of the Virgo detector during its second science run, 2011, https://arxiv.org/pdf/1009.5190.pdf

A Monitoring of Hrec/Hinj during O3: all plots

The O3 run was done in two parts: O3a (from 2020-04-01 to 2020-09-30) and O3b (from 2020-11-01 to 2021-03-27). For each of those parts, an estimation of the $h(t)$ uncertainty has been done using the transfer functions hrec/hinj computed by TFMoni.

O3a: Plots for the modulus of the transfer function between the reconstructed h(t) and NE or WE hinj, at various frequencies, during O3a are shown in Figures 10 and 11.
Plots for the phase of the transfer function between the reconstructed $h(t)$ and NE or WE hinj, at various frequencies, during O3a are shown in Figures 12 and 13. The TFMoni data used to do these plots have been reprocessed at CCin2p3 and a few days of data are missing. This does not change the result.

O3b: Plots for the modulus of the transfer function between the reconstructed $h(t)$ and NE or WE hinj, at various frequencies, during O3b are shown in Figures 14 and 15.
Plots for the phase of the transfer function between the reconstructed $h(t)$ and NE or WE hinj, at various frequencies, during O3b are shown in Figures 16 and 17. The TFMoni data used to do these plots have been reprocessed on Virgo site.

The following data samples have been excluded from the plots:

1. coherence associated to the transfer function is below 0.98
2. Virgo interferometer is not in science mode
3. Virgo interferometer is in science mode since less than 1200 s. This very conservative window excludes start of averaging of TF by TFMoni after the relock.
4. Virgo interferometer is 300 s before the end of science mode. This cut allows to exclude possible noisier interferometer before an unlock.
5. PCal channel is used by TFMoni but PCal power is below 1.8 W (PCal not working)
6. In the previous 900 seconds, the BNS range was, at least one time, below 30 Mpc (a glitch occured). This allow to exclude TFMoni recovering period after a large glitch occured that corrupted the averaged FFTs.
7. TFMoni data is missing
8. The modulus value provided by TFMoni is below 0.01 (which means that it was not computed)
9. The phase value provided by TFMoni is below -3.2 rad (which means that it was not computed)

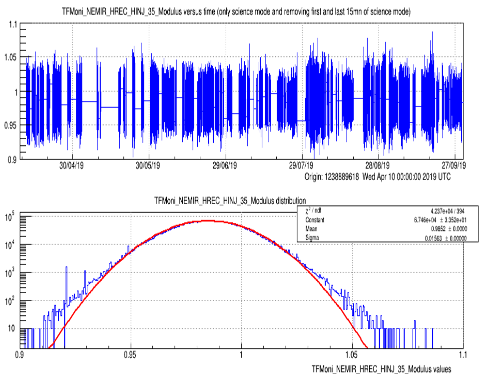

(a) O3a, modulus, NE EM, ∼35 Hz

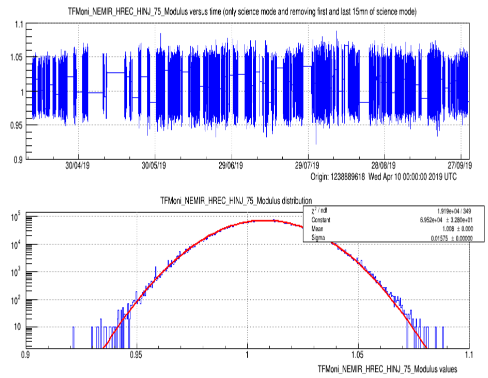

(b) O3a, modulus, NE EM, ∼75 Hz

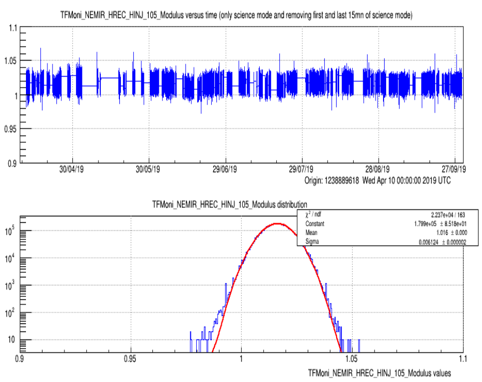

(c) O3a, modulus, NE EM, ∼105 Hz

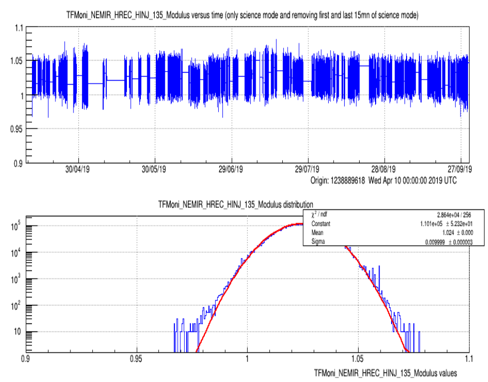

(d) O3a, modulus, NE EM, ∼135 Hz

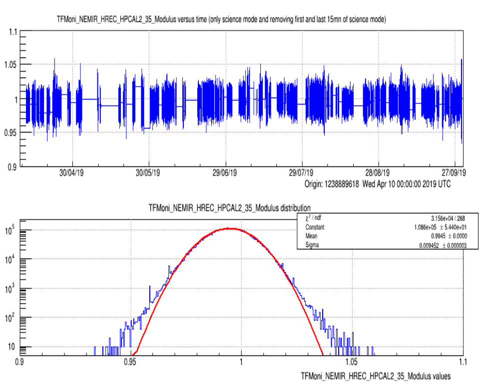

(e) O3a, modulus, NE PCal, ∼35 Hz

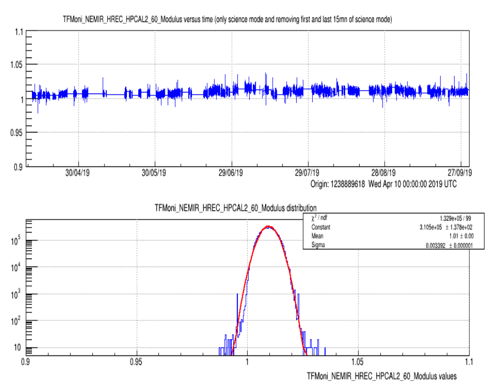

(f) O3a, modulus, NE PCal, ∼60 Hz

Figure 10: TFMoni Modulus of the transfer function between reconstructed h(t) and NE hinj or NE PCal (last two plots), during O3a, at the frequencies of the NE injected permanent lines. For each plot, time evolution and fitted distribution are shown.

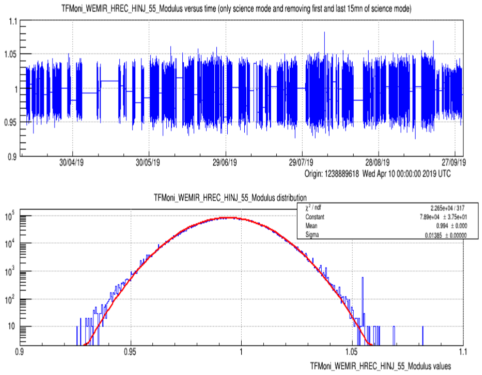

(a) O3a, modulus, WE EM, ∼35 Hz

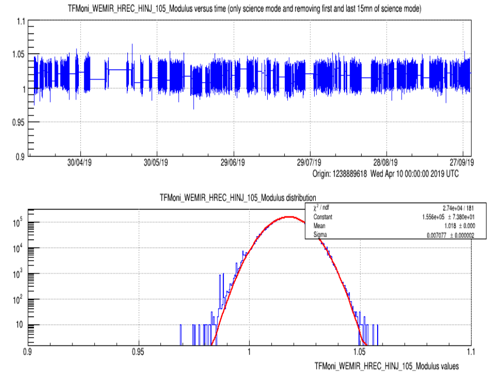

(b) O3a, modulus, WE EM, ∼105 Hz

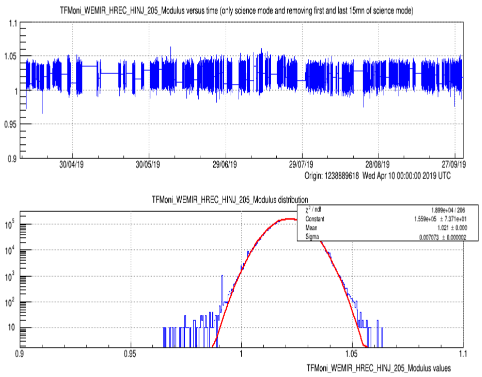

(c) O3a, modulus, WE EM, ∼205 Hz

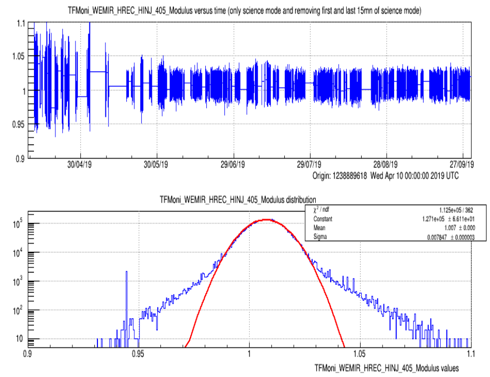

(d) O3a, modulus, WE EM, ∼405 Hz

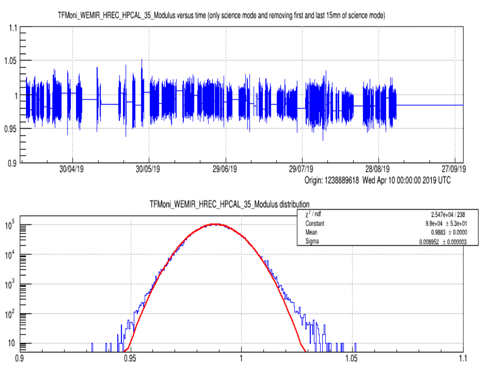

(e) O3a, modulus, WE PCal, ∼35 Hz
(WE PCal not working in Sept. 2019)

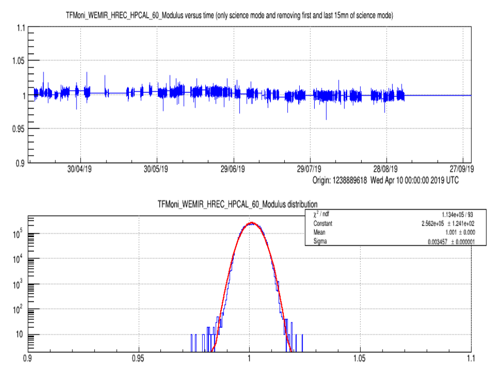

(f) O3a, modulus, WE PCal, ∼60 Hz
(WE PCal not working in Sept. 2019)

Figure 11: TFMoni Modulus of the transfer function between reconstructed h(t) and WE hinj or WE PCal (last two plots), during O3a, at the frequencies of the WE injected permanent lines. For each plot, time evolution and fitted distribution are shown.

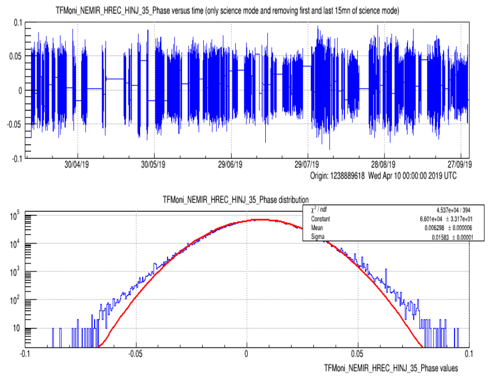

(a) O3a, phase, NE EM, ∼35 Hz

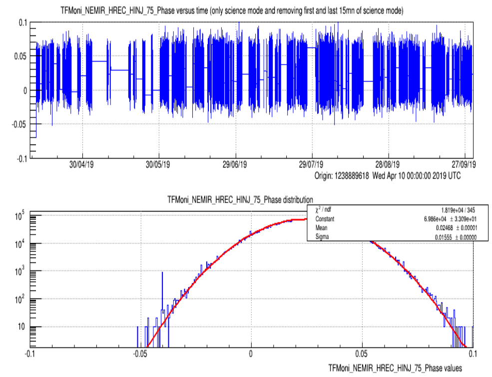

(b) O3a, phase, NE EM, ∼75 Hz

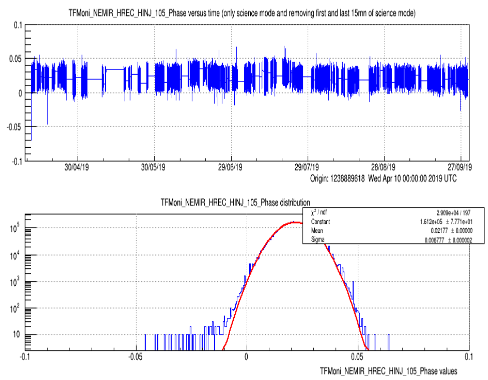

(c) O3a, phase, NE EM, ∼105 Hz

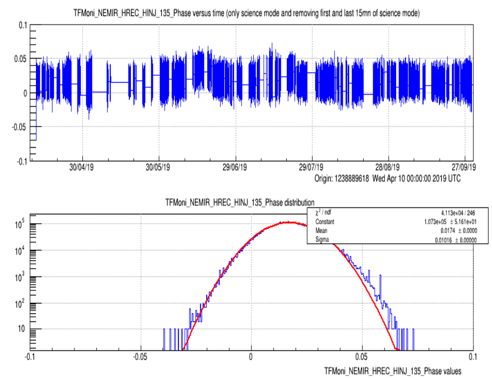

(d) O3a, phase, NE EM, ∼135 Hz

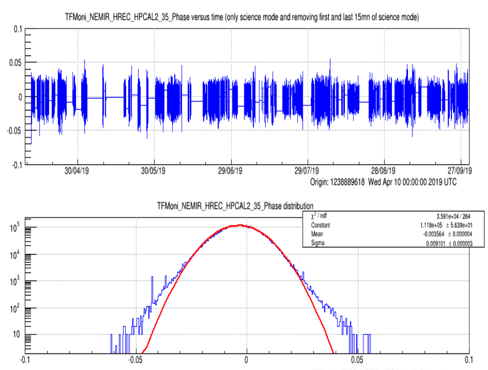

(e) O3a, phase, NE PCal, ∼35 Hz

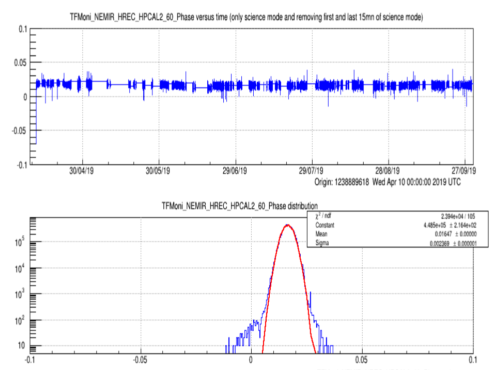

(f) O3a, phase, NE PCal, ∼60 Hz

Figure 12: TFMoni Phase of the transfer function between reconstructed h(t) and NE hinj or NE PCal (last two plots) , during O3a, at the frequencies of the NE injected permanent lines. For each plot, time evolution and fitted distribution are shown.

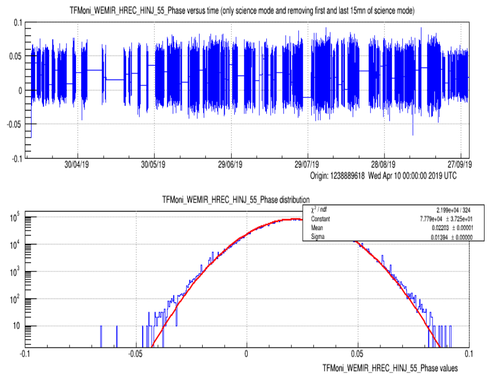

(a) O3a, phase, WE EM, ∼55 Hz

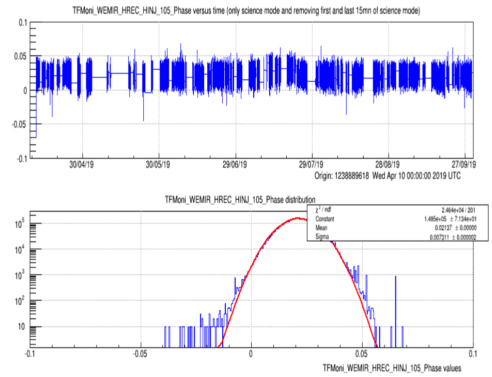

(b) O3a, phase, WE EM, ∼105 Hz

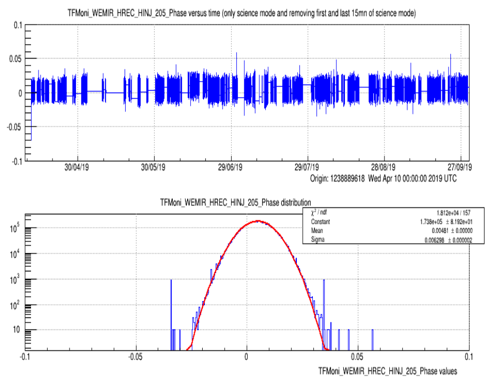

(c) O3a, phase, WE EM, ∼205 Hz

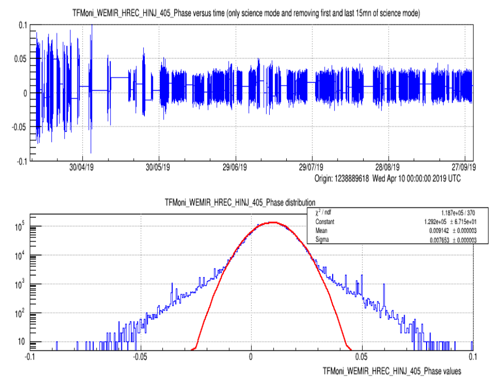

(d) O3a, phase, WE EM, ∼405 Hz

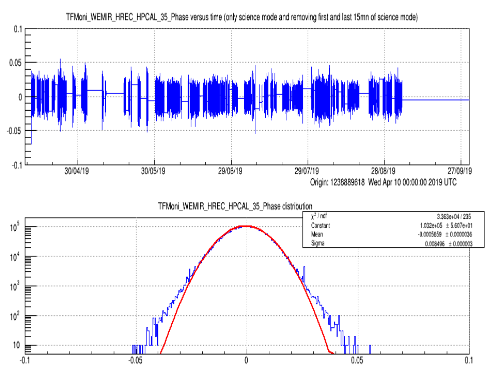

(e) O3a, phase, WE PCal, ∼35 Hz
(WE PCal not working in Sept. 2019)

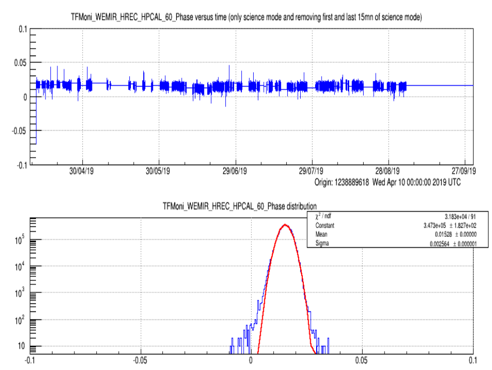

(f) O3a, phase, WE PCal, ∼60 Hz
(WE PCal not working in Sept. 2019)

Figure 13: TFMoni Phase of the transfer function between reconstructed h(t) and WE hinj or WE PCal (last two plots), during O3a, at the frequencies of the WE injected permanent lines. For each plot, time evolution and fitted distribution are shown.

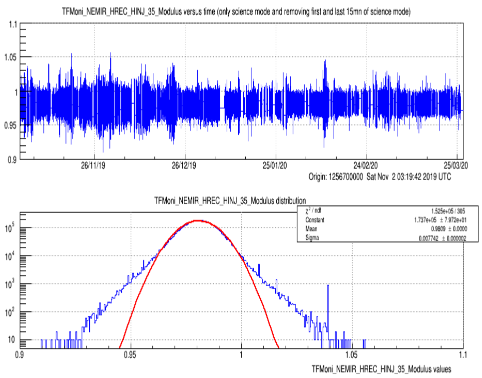

(a) O3b, modulus, NE EM, ∼35 Hz

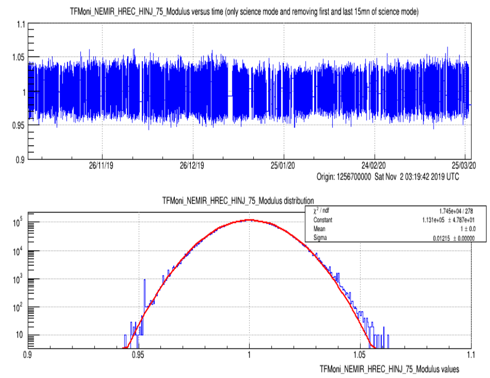

(b) O3b, modulus, NE EM, ∼75 Hz

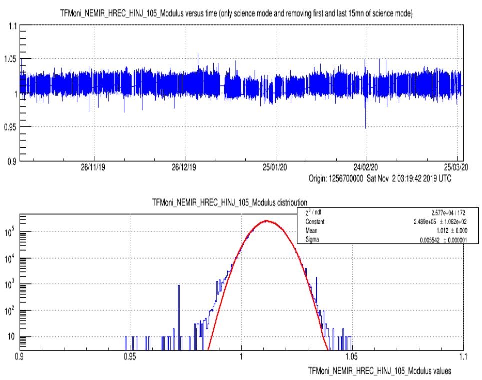

(c) O3b, modulus, NE EM, ∼105 Hz

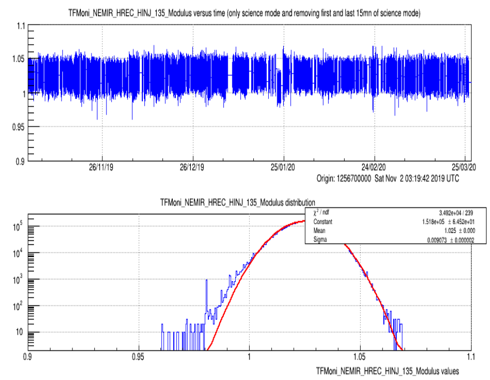

(d) O3b, modulus, NE EM, ∼135 Hz

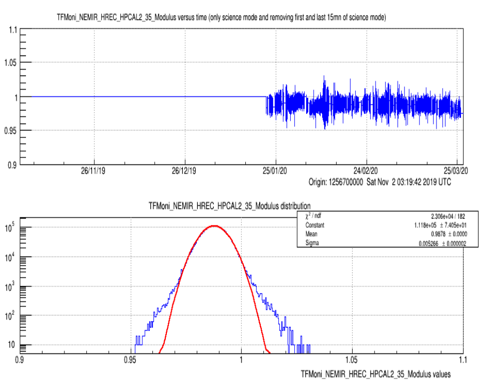

(e) O3b, modulus, NE PCal, ∼35 Hz
(NE PCal not working until end January 2020)

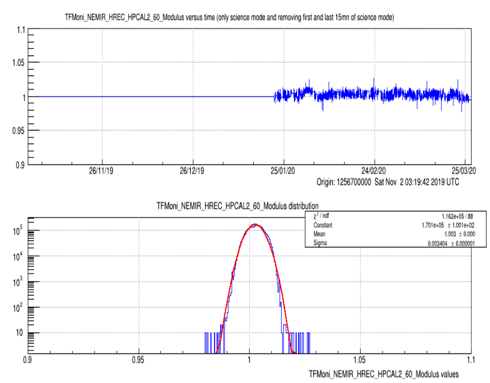

(f) O3b, modulus, NE PCal, ∼60 Hz
(NE PCal not working until end January 2020)

Figure 14: TFMoni Modulus of the transfer function between reconstructed h(t) and NE hinj or NE PCal (last two plots), during O3a, at the frequencies of the NE injected permanent lines. For each plot, time evolution and fitted distribution are shown.

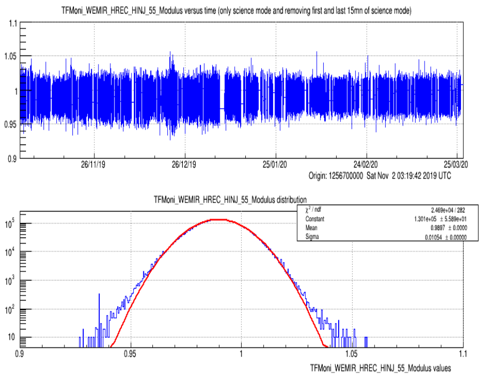

(a) O3b, modulus, WE EM, ∼55 Hz

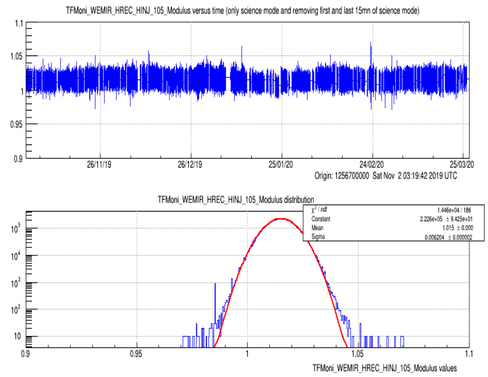

(b) O3b, modulus, WE EM, ∼105 Hz

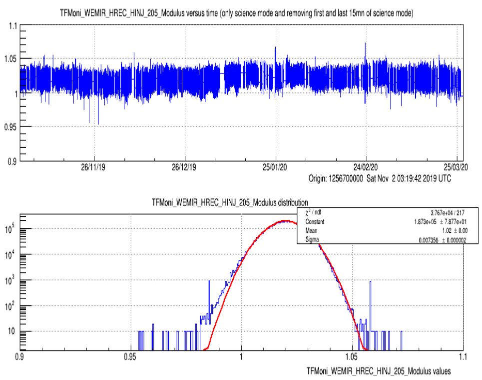

(c) O3b, modulus, WE EM, ∼205 Hz

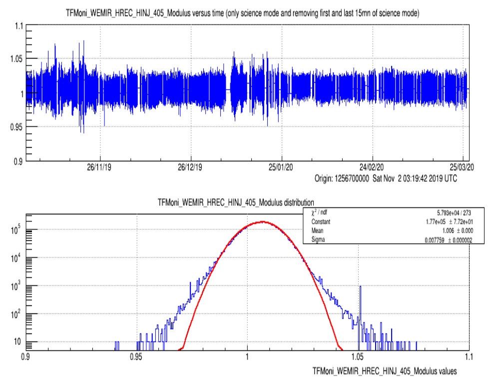

(d) O3b, modulus, WE EM, ∼405 Hz

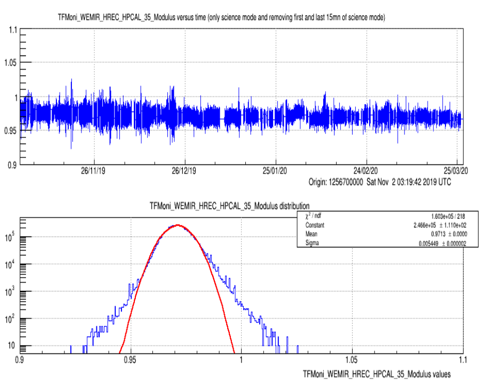

(e) O3b, modulus, WE PCal, ∼35 Hz

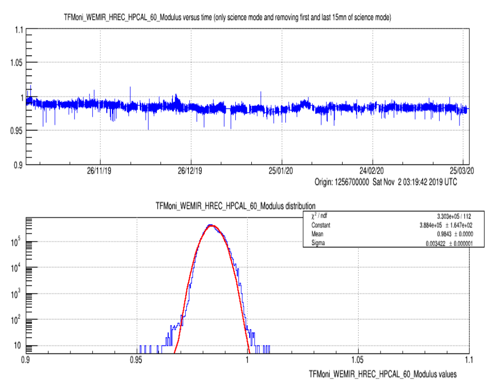

(f) O3b, modulus, WE PCal, ∼60 Hz

Figure 15: TFMoni Modulus of the transfer function between reconstructed h(t) and WE hinj or WE PCal (last two plots), during O3a, at the frequencies of the WE injected permanent lines. For each plot, time evolution and fitted distribution are shown.

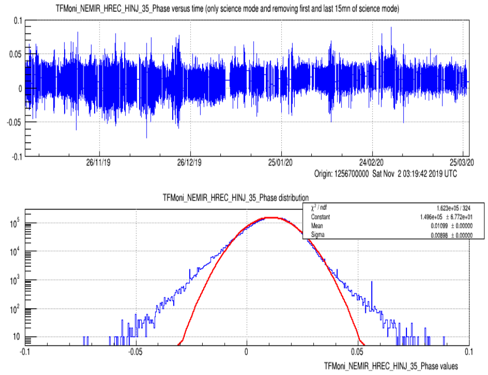

(a) O3b, phase, NE EM, ∼35 Hz

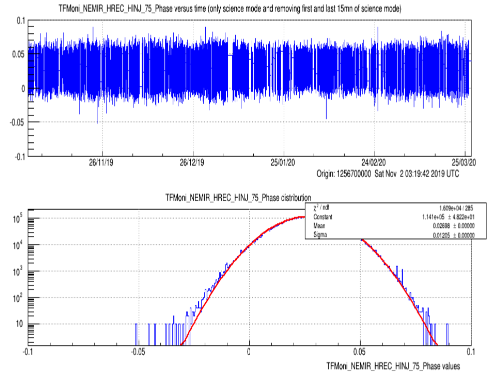

(b) O3b, phase, NE EM, ∼75 Hz

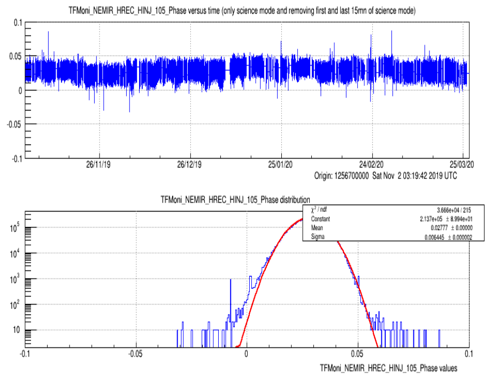

(c) O3b, phase, NE EM, ∼105 Hz

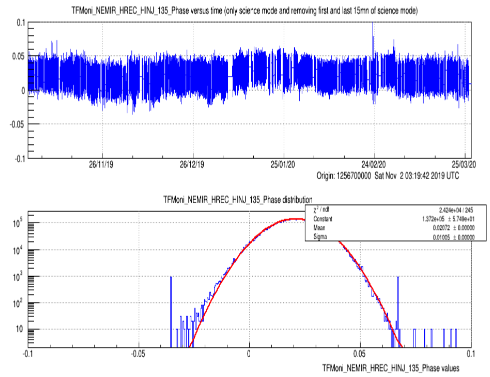

(d) O3b, phase, NE EM, ∼135 Hz

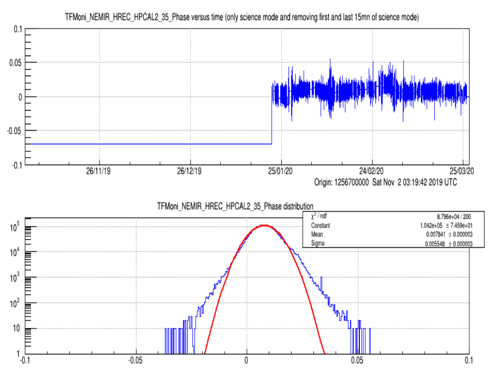

(e) O3b, phase, NE PCal, ∼35 Hz
(NE PCal not working until end January 2020)

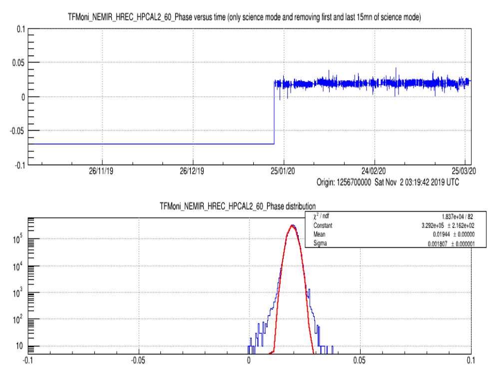

(f) O3b, phase, NE PCal, ∼60 Hz
(NE PCal not working until end January 2020)

Figure 16: TFMoni Phase of the transfer function between reconstructed h(t) and NE hinj or NE PCal (last two plots) , during O3a, at the frequencies of the NE injected permanent lines. For each plot, time evolution and fitted distribution are shown.

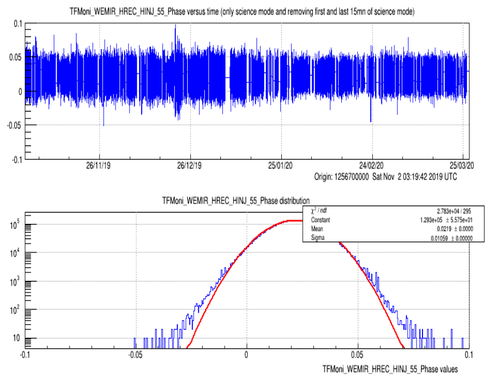

(a) O3b, phase, WE EM, ∼55 Hz

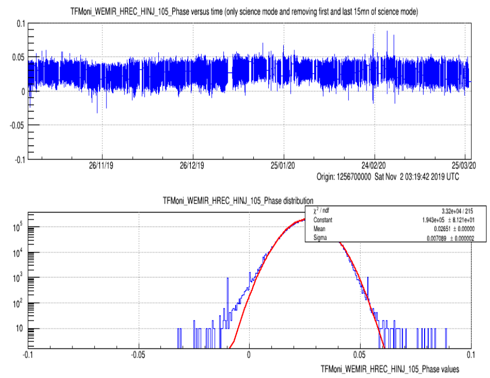

(b) O3b, phase, WE EM, ∼105 Hz

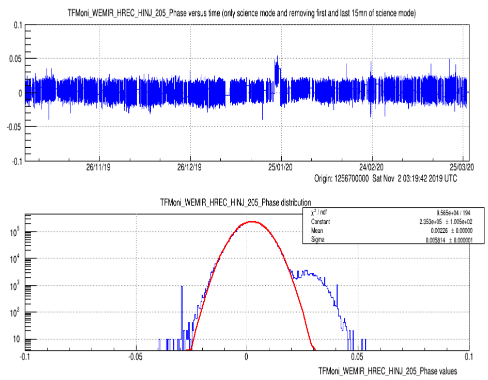

(c) O3b, phase, WE EM, ∼205 Hz

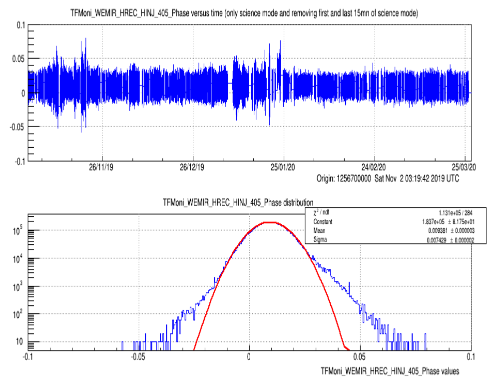

(d) O3b, phase, WE EM, ∼405 Hz

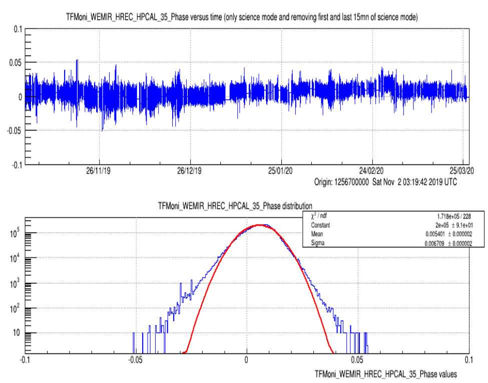

(e) O3b, phase, WE PCal, ∼35 Hz

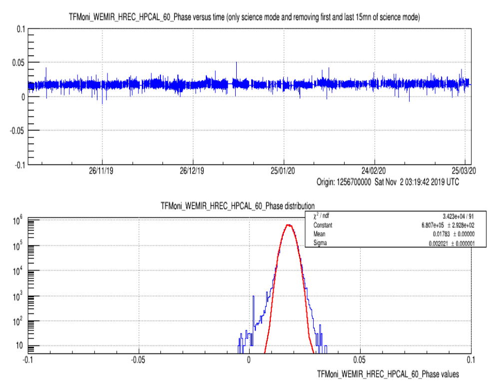

(f) O3b, phase, WE PCal, ∼60 Hz

Figure 17: TFMoni Phase of the transfer function between reconstructed h(t) and WE hinj or WE PCal (last two plots), during O3a, at the frequencies of the WE injected permanent lines. For each plot, time evolution and fitted distribution are shown.

A Monitoring of coils voltage during O3: all plots

Plots for the Modulus near 60 Hz of the transfer function between the coil voltage and the control loop signal are shown in Figures 18 , 19 , 20 and 21. Plots for the Modulus near 355 Hz of the transfer function between the coil voltage and the control loop signal are shown in Figures 22 , 23 , 24 and 25.

Plots for the Phase near 60 Hz of the transfer function between the coil voltage and the control loop signal are shown in Figures 26 , 27 , 28 and 29. Plots for the Phase near 355 Hz of the transfer function between the coil voltage and the control loop signal are shown in Figures 30 , 31 , 32 and 33.

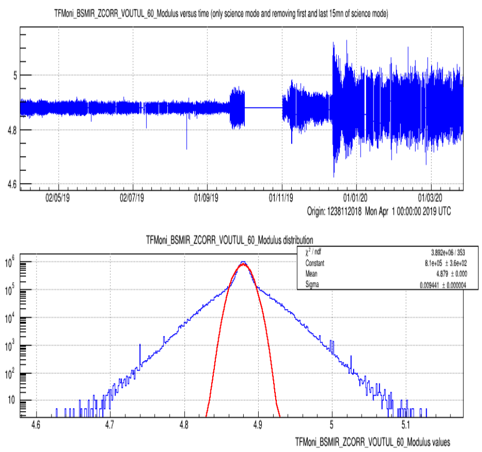

(a) BS, VOUT_UL

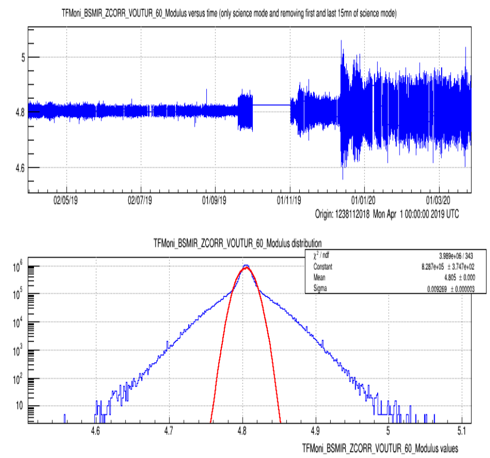

(b) modulus BS, VOUT_UR , ~60 Hz

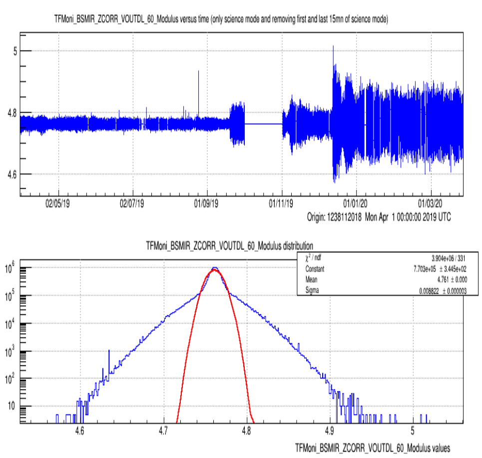

(c) modulus BS, VOUT_DL , ~60 Hz

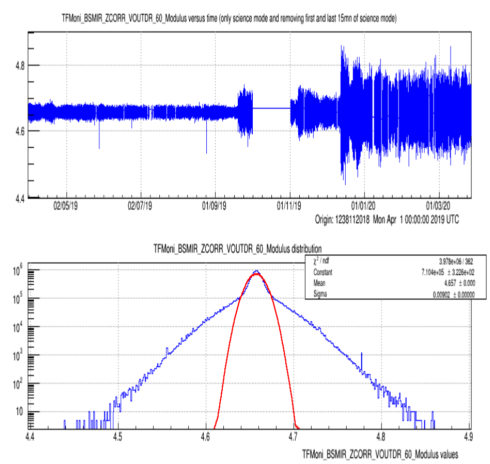

(d) modulus BS, VOUT_DR , ~60 Hz

Figure 18: TFMoni Modulus near 60 Hz of the transfer function between BS coil voltages VOUT_DL, VOUT_DR, VOUT_UL and VOUT_UR and the longitudinal control loop signals Sc_BS_MIR_Z_CORR. For each plot, time evolution and fitted distribution are shown. By mistake in TFMoni configuration, for BS and PR, the online TF was not computed at the frequency of the injected line. Thus, the uncertainty on modulus and phase may differ from the one that would have been measured at the line frequency. Moreover, during O3b, the control signals were reduced, low enough so that the coils current monitoring was close to the sensing noise. As a consequence, the coherence between the two signals involved in the TF was reduced, hence the statistical fluctuations of the TF increased.

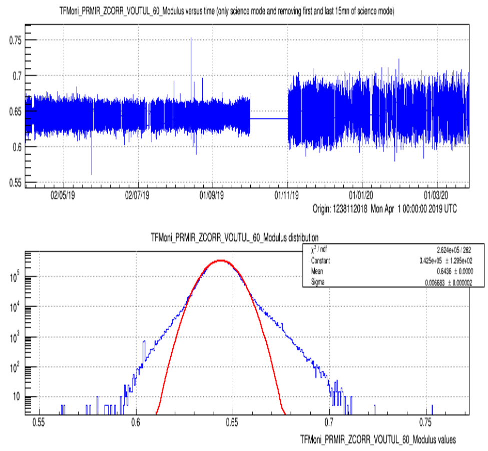

(a) modulus PR, VOUT_UL, ~60 Hz

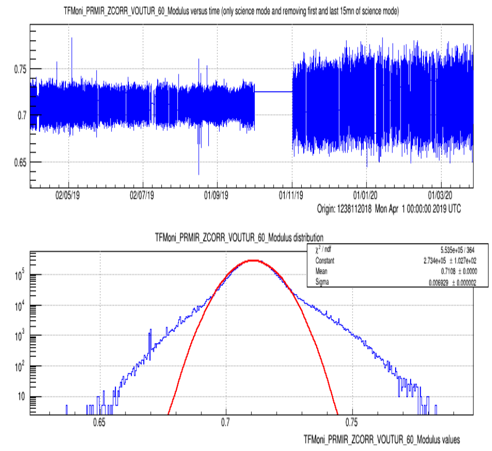

(b) modulus PR, VOUT_UR, ~60 Hz

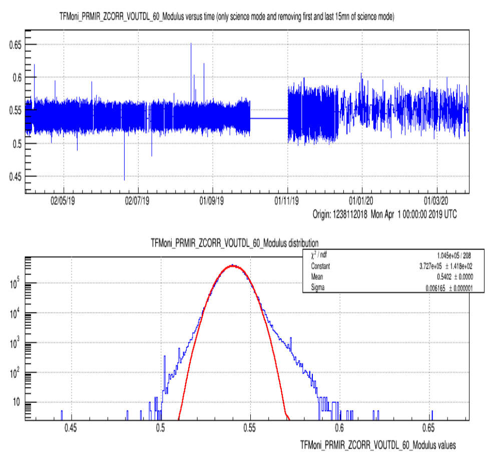

(c) modulus PR, VOUT_DL, ~60 Hz

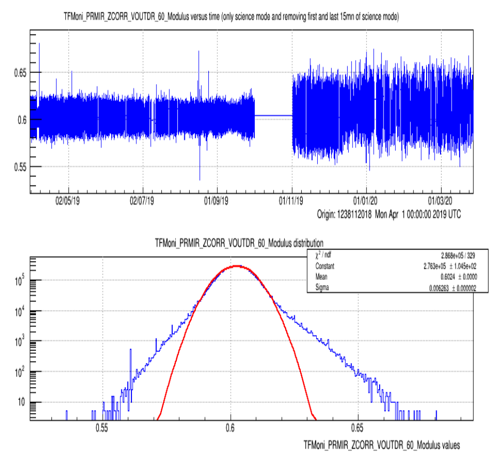

(d) modulus PR, VOUT_DR , ~60 Hz

Figure 19: TFMoni Modulus near 60 Hz of the transfer function between PR coil voltages VOUT_UL, VOUT_UR, VOUT_DL and VOUT_DR and the longitudinal control loop signals Sc_PR_MIR_Z_CORR. For each plot, time evolution and fitted distribution are shown. By mistake in TFMoni configuration, for BS and PR, the online TF was not computed at the frequency of the injected line. Thus, the uncertainty on modulus and phase may differ from the one that would have been measured at the line frequency. Moreover, during O3b, the control signals were reduced, low enough so that the coils current monitoring was close to the sensing noise. As a consequence, the coherence between the two signals involved in the TF was reduced, hence the statistical fluctuations of the TF increased.

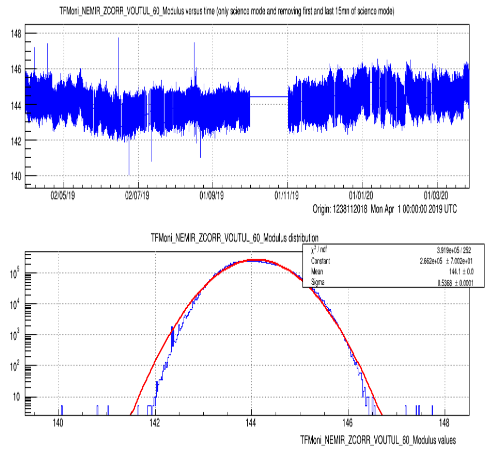

(a) modulus NE, VOUT_UL, ∼60 Hz

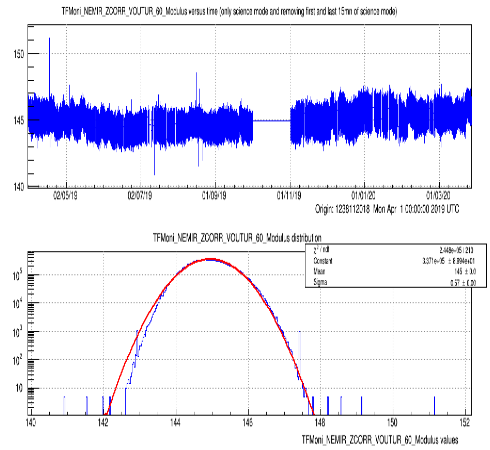

(b) modulus NE, VOUT_UR, ∼60 Hz

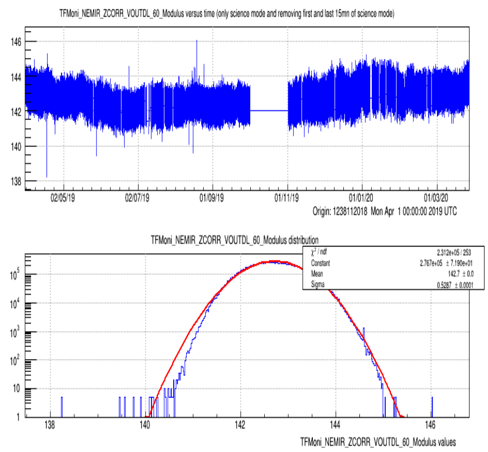

(c) modulus NE, VOUT_DL, ∼60 Hz

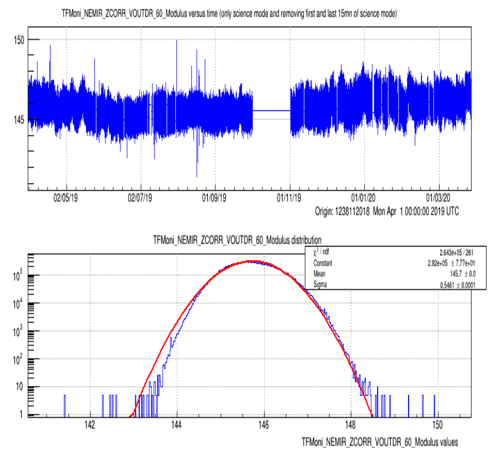

(d) modulus NE, VOUT_DR, ∼60 Hz

Figure 20: TFMoni Modulus near 60 Hz of the transfer function between NE coil voltages VOUT_UL, VOUT_UR, VOUT_DL and VOUT_DR and the longitudinal control loop signals Sc_NE_MIR_Z_CORR. For each plot, time evolution and fitted distribution are shown.

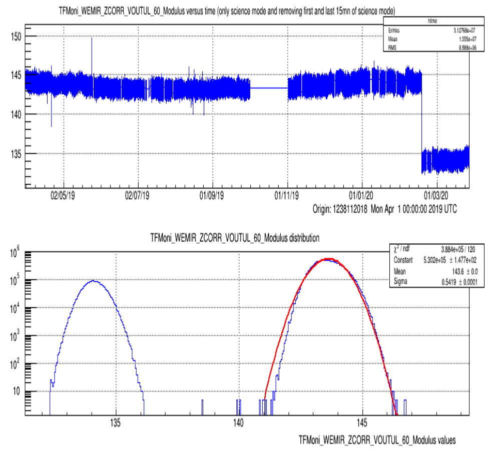

(a) modulus WE, VOUT_UL, ∼60 Hz

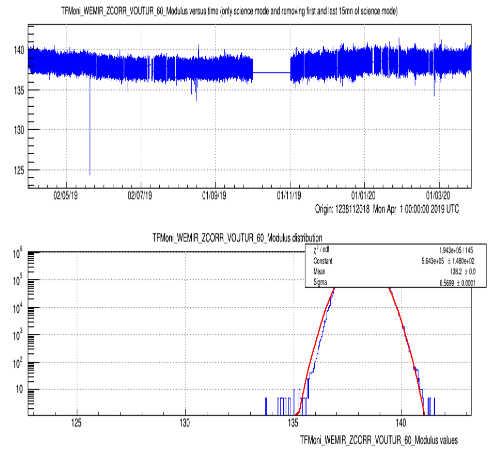

(b) modulus WE, VOUT_UR, ∼60 Hz

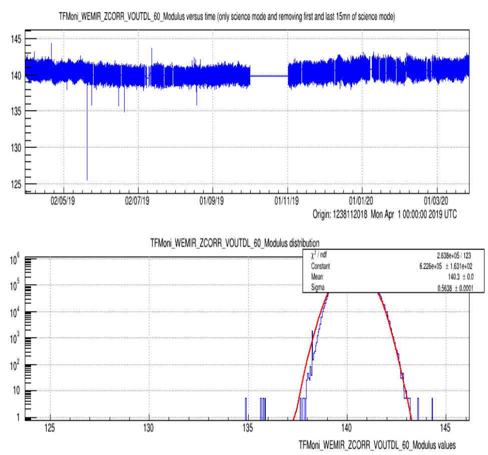

(c) modulus WE, VOUT_DL, ∼60 Hz

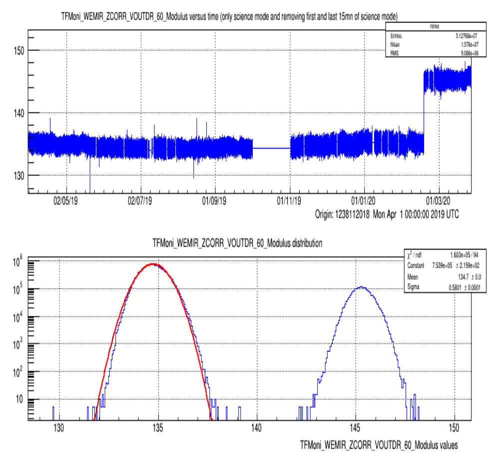

(d) modulus WE, VOUT_DR, ∼60 Hz

Figure 21: TFMoni Modulus near 60 Hz of the transfer function between WE coil voltages VOUT_UL, VOUT_UR, VOUT_DL and VOUT_DR and the longitudinal control loop signals Sc_WE_MIR_Z_CORR. For each plot, time evolution and fitted distribution are shown. On February 18th 2020, some cabling was rearranged on WE mirror actuator and the driving matrix was updated accordingly in the DSP (see https://logbook.virgo-gw.eu/virgo/?r=48483). This explains why the values were suddenly exchanged between UL and DR. However, this added no impact on the WE actuator's response.

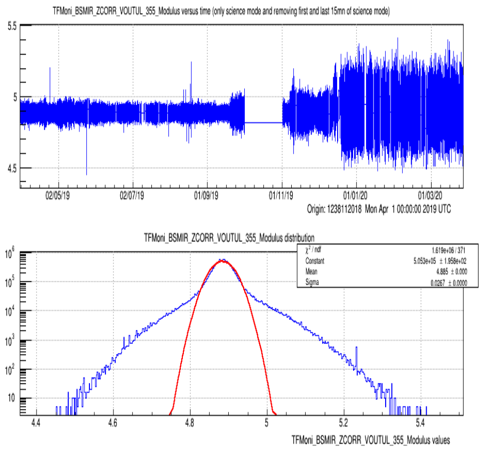

(a) modulus BS, VOUT_UL , ∼355 Hz

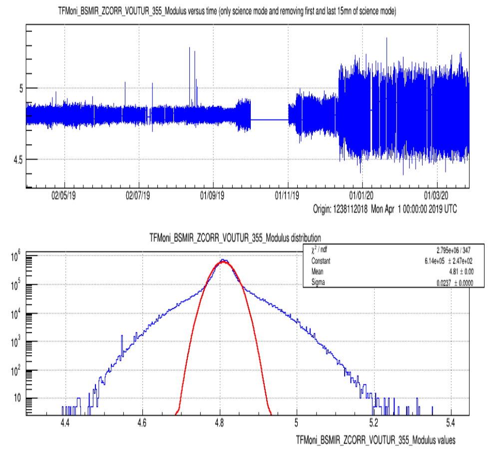

(b) modulus BS, VOUT_UR , ∼355 Hz

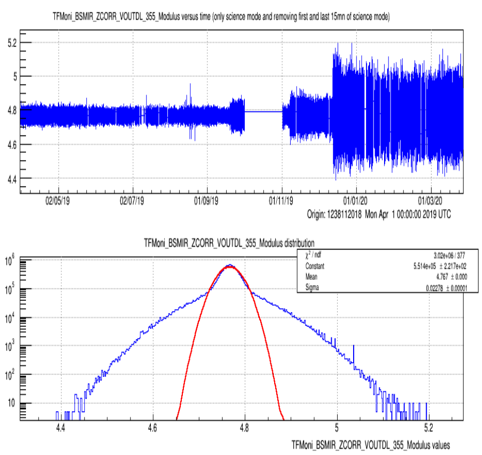

(c) modulus BS, VOUT_DL , ∼355 Hz

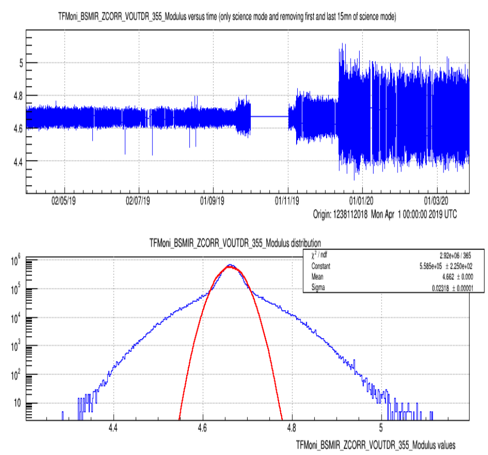

(d) modulus BS, VOUT_DR , ∼355 Hz

Figure 22: TFMoni Modulus near 355 Hz of the transfer function between BS coil voltages VOUT_UL, VOUT_UR, VOUT_DL and VOUT_DR and the longitudinal control loop signals Sc_BS_MIR_Z_CORR. For each plot, time evolution and fitted distribution are shown. By mistake in TFMoni configuration, for BS and PR, the online TF was not computed at the frequency of the injected line. Thus, the uncertainty on modulus and phase may differ from the one that would have been measured at the line frequency. Moreover, during O3b, the control signals were reduced, low enough so that the coils current monitoring was close to the sensing noise. As a consequence, the coherence between the two signals involved in the TF was reduced, hence the statistical fluctuations of the TF increased.

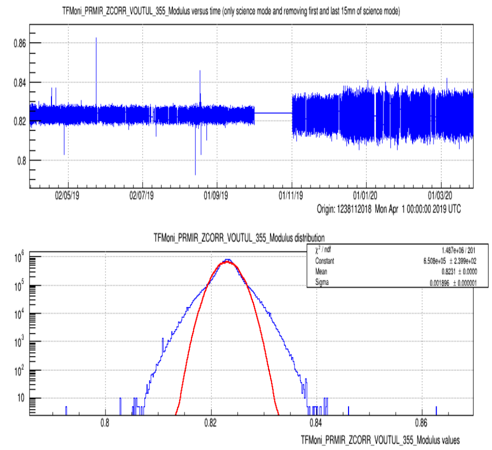

(a) modulus PR, VOUT_UL , ∼355 Hz

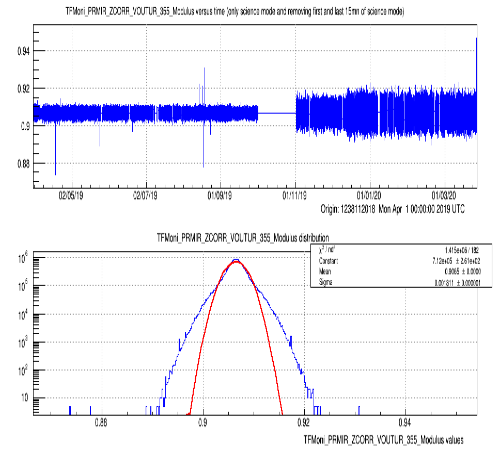

(b) modulus PR, VOUT_UR , ∼355 Hz

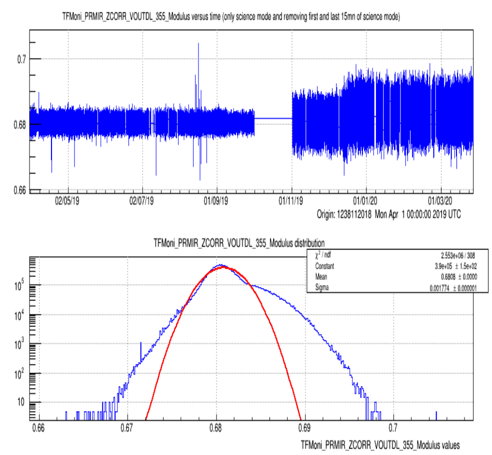

(c) modulus PR, VOUT_DL , ∼355 Hz

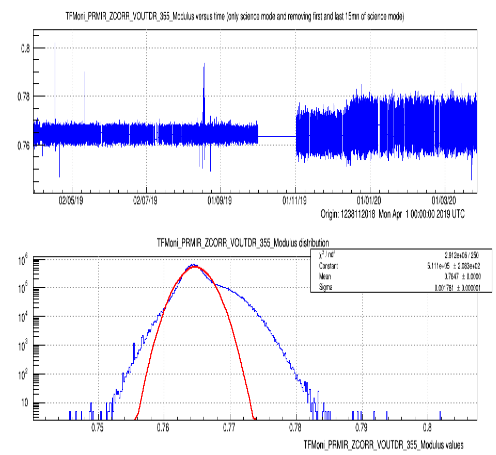

(d) modulus PR, VOUT_DR , ∼355 Hz

Figure 23: TFMoni Modulus near 355 Hz of the transfer function between PR coil voltages VOUT_UL, VOUT_UR, VOUT_DL and VOUT_DR and the longitudinal control loop signals Sc_PR_MIR_Z_CORR. For each plot, time evolution and fitted distribution are shown. By mistake in TFMoni configuration, for BS and PR, the online TF was not computed at the frequency of the injected line. Thus, the uncertainty on modulus and phase may differ from the one that would have been measured at the line frequency. Moreover, during O3b, the control signals were reduced, low enough so that the coils current monitoring was close to the sensing noise. As a consequence, the coherence between the two signals involved in the TF was reduced, hence the statistical fluctuations of the TF increased.

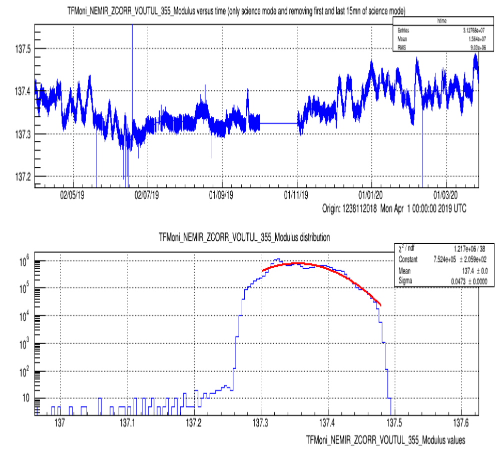

(a) modulus NE, VOUT_UL , ∼355 Hz

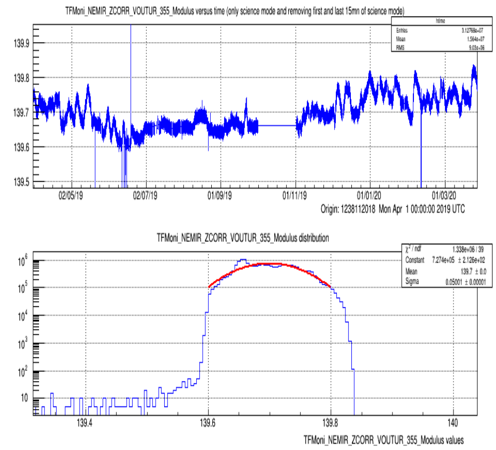

(b) modulus NE, VOUT_UR , ∼355 Hz

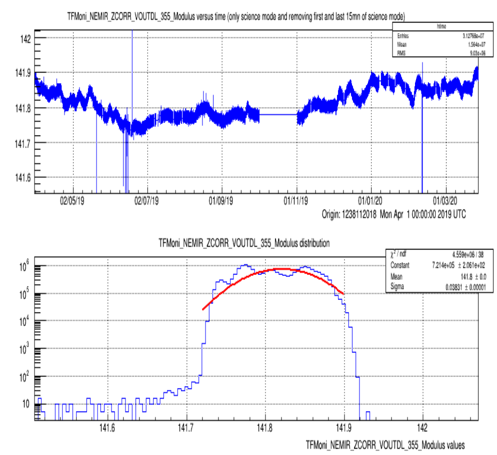

(c) modulus NE, VOUT_DL , ∼355 Hz

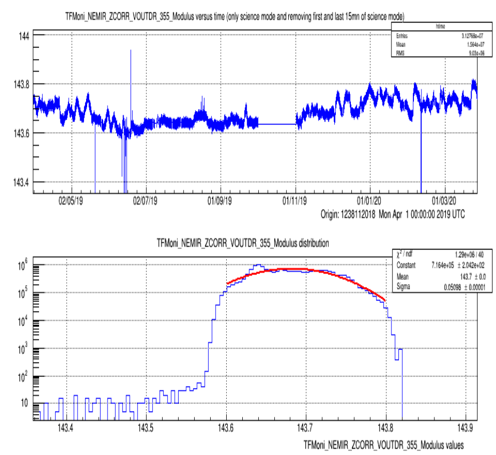

(d) modulus NE, VOUT_DR , ∼355 Hz

Figure 24: TFMoni Modulus near 355 Hz of the transfer function between NE coil voltages VOUT_UL, VOUT_UR, VOUT_DL and VOUT_DR and the longitudinal control loop signals Sc_NE_MIR_Z_CORR. For each plot, time evolution and fitted distribution are shown. Around 355 Hz, the fluctuations on the modulus of NE, even small, are not Gaussian and show various trends over days or weeks.

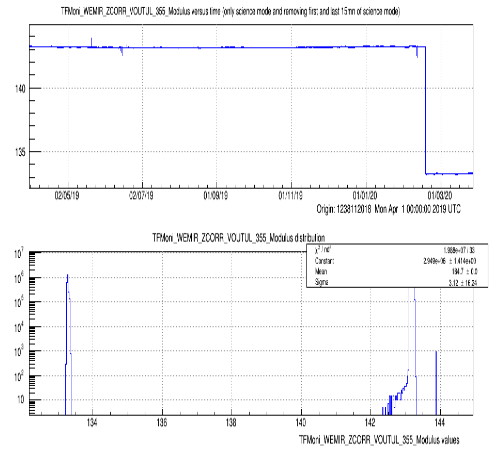

(a) modulus WE, VOUT_UL , ∼355 Hz

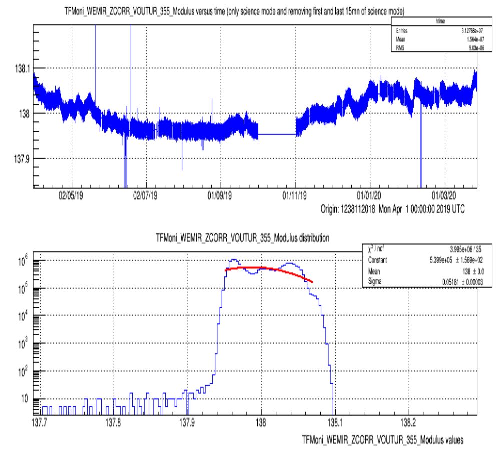

(b) modulus WE, VOUT_UR , ∼355 Hz

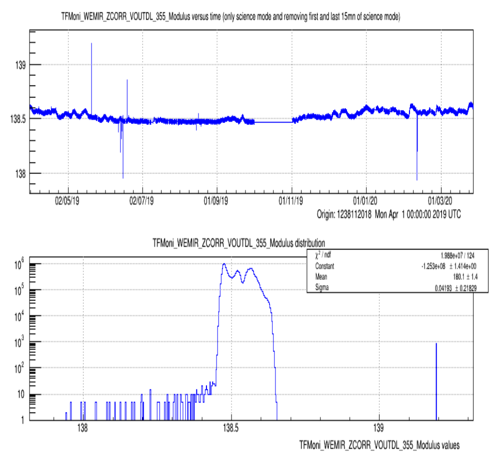

(c) modulus WE, VOUT_DL , ∼355 Hz

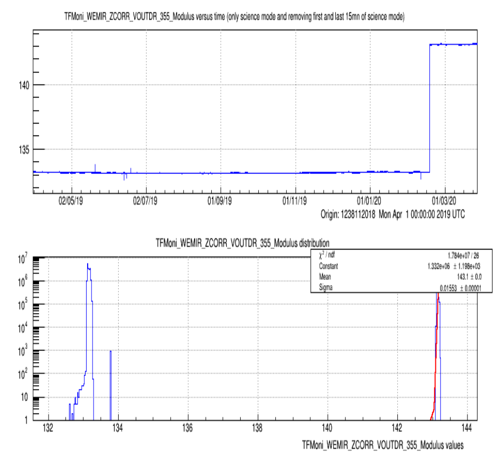

(d) modulus WE, VOUT_DR , ∼355 Hz

Figure 25: TFMoni Modulus near 355 Hz of the transfer function between WE coil voltages VOUT_UL, VOUT_UR, VOUT_DL and VOUT_DR and the longitudinal control loop signals Sc_WE_MIR_Z_CORR. For each plot, time evolution and fitted distribution are shown. On February 18th 2020, some cabling was rearranged on WE mirror actuator and the driving matrix was updated accordingly in the DSP (see https://logbook.virgo-gw.eu/virgo/?r=48483). But maybe the sensing was not changed, which explains why the values were exchanged between UL and DR. This added no impact on the actuator's response. Around 355 Hz, the fluctuations on the modulus of WE, even small, are not Gaussian and show various trends over days or weeks.

Below are the plots for the Phase near 60 Hz and near 355 Hz of the TF between the coil voltages and the longitudinal control signals.

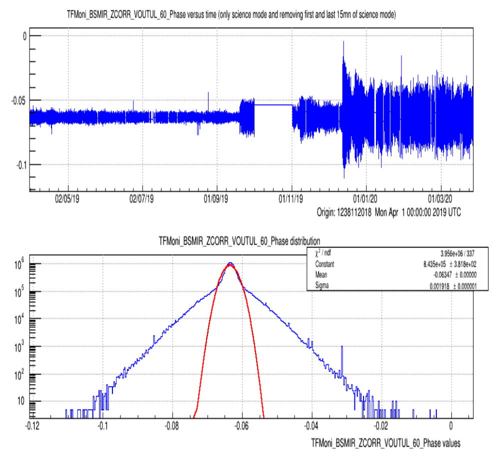

(a) phase BS, VOUT_UL , ∼60 Hz

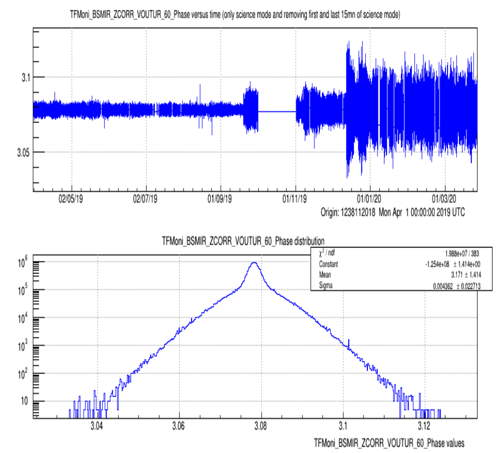

(b) phase BS, VOUT_UR , ∼60 Hz

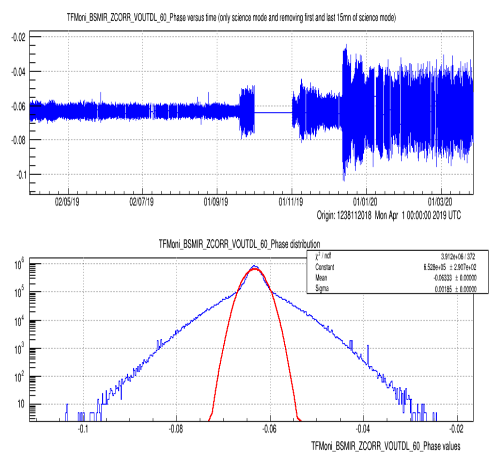

(c) phase BS, VOUT_DL , ∼60 Hz

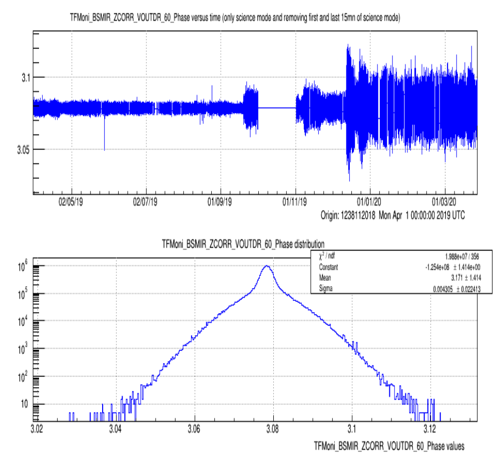

(d) phase BS, VOUT_DR , ∼60 Hz

Figure 26: TFMoni Phase near 60 Hz of the transfer function between BS coil voltages VOUT_UL, VOUT_UR, VOUT_DL and VOUT_DR and the longitudinal control loop signals Sc_BS_MIR_Z_CORR. For each plot, time evolution and fitted distribution are shown. By mistake in TFMoni configuration, for BS and PR, the online TF was not computed at the frequency of the injected line. Thus, the uncertainty on modulus and phase may differ from the one that would have been measured at the line frequency. Moreover, during O3b, the control signals were reduced, low enough so that the coils current monitoring was close to the sensing noise. As a consequence, the coherence between the two signals involved in the TF was reduced, hence the statistical fluctuations of the TF increased.

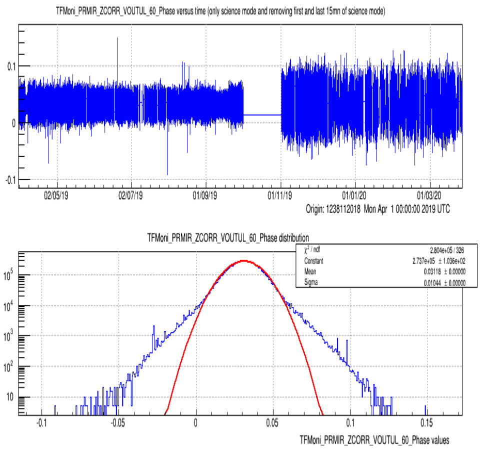

(a) phase PR, VOUT_UL , ∼60 Hz

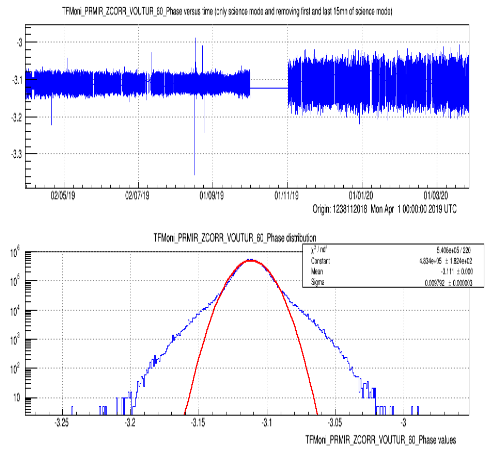

(b) phase PR, VOUT_UR , ∼60 Hz

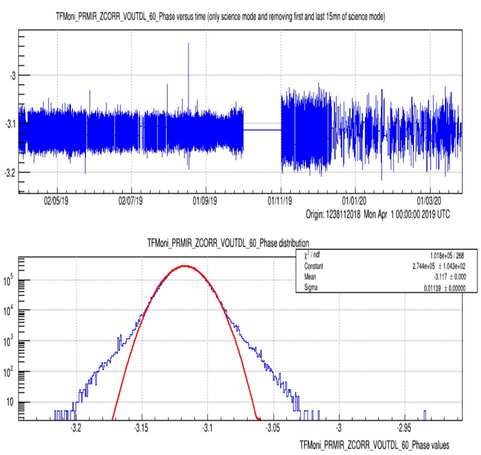

(c) phase PR, VOUT_DL , ∼60 Hz

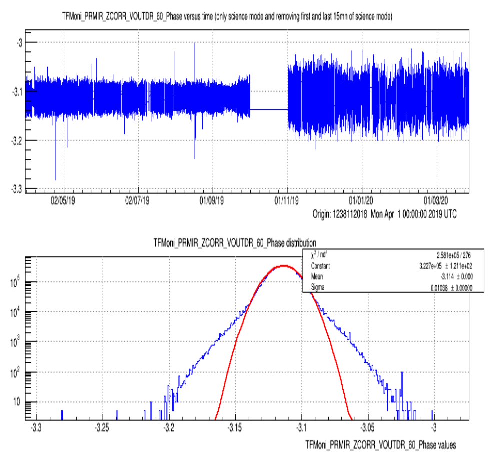

(d) phase PR, VOUT_DR , ∼60 Hz

Figure 27: TFMoni Phase near 60 Hz of the transfer function between PR coil voltages VOUT_UL, VOUT_UR, VOUT_DL and VOUT_DR and the longitudinal control loop signals Sc_PR_MIR_Z_CORR. For each plot, time evolution and fitted distribution are shown. By mistake in TFMoni configuration, for BS and PR, the online TF was not computed at the frequency of the injected line. Thus, the uncertainty on modulus and phase may differ from the one that would have been measured at the line frequency. Moreover, during O3b, the control signals were reduced, low enough so that the coils current monitoring was close to the sensing noise. As a consequence, the coherence between the two signals involved in the TF was reduced, hence the statistical fluctuations of the TF increased.

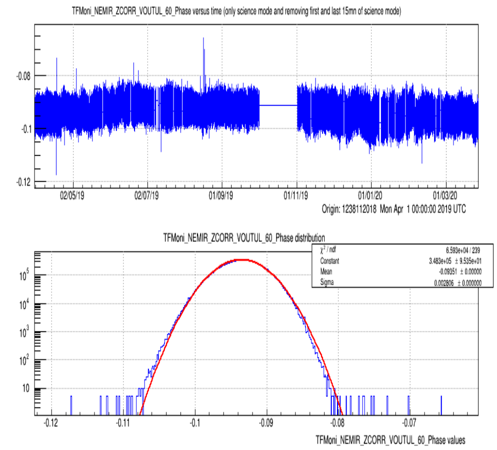

(a) phase NE, VOUT_UL , ∼60 Hz

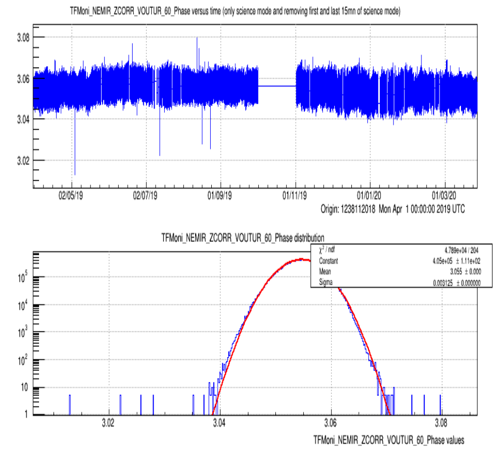

(b) phase NE, VOUT_UR , ∼60 Hz

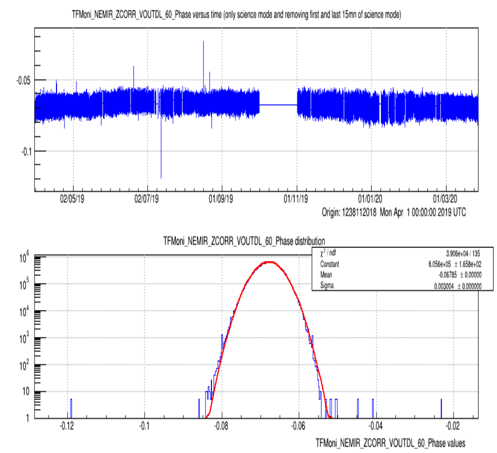

(c) phase NE, VOUT_DL , ∼60 Hz

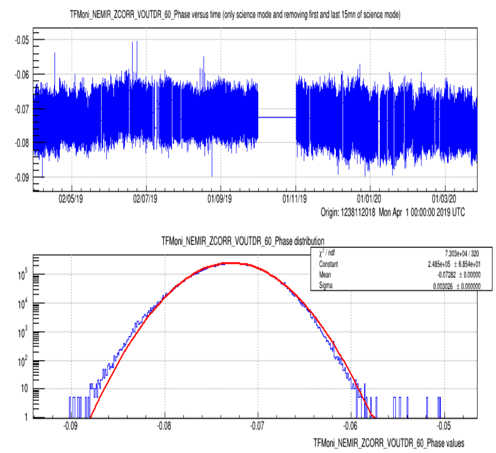

(d) phase NE, VOUT_DR , ∼60 Hz

Figure 28: TFMoni Phase near 60 Hz of the transfer function between NE coil voltages VOUT_UL, VOUT_UR, VOUT_DL and VOUT_DR and the longitudinal control loop signals Sc_NE_MIR_Z_CORR. For each plot, time evolution and fitted distribution are shown.

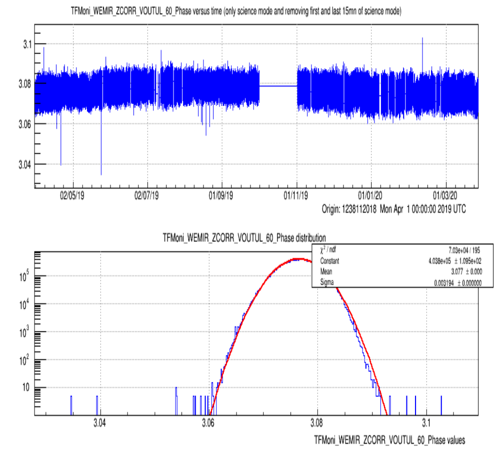

(a) phase WE, VOUT_UL , ∼60 Hz

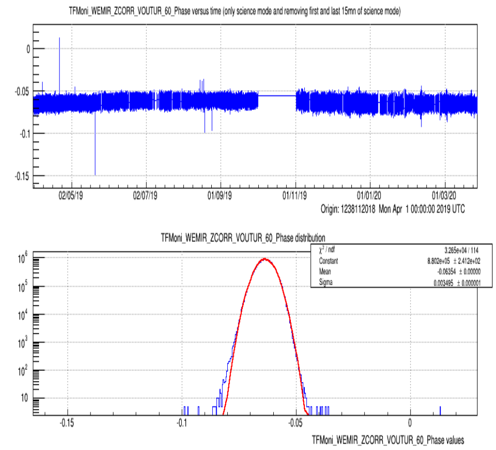

(b) phase WE, VOUT_UR , ∼60 Hz

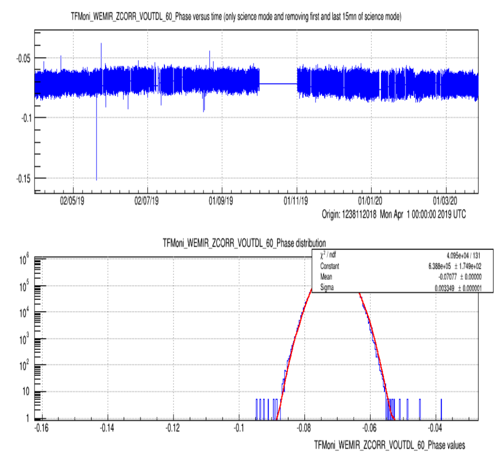

(c) phase WE, VOUT_DL , ∼60 Hz

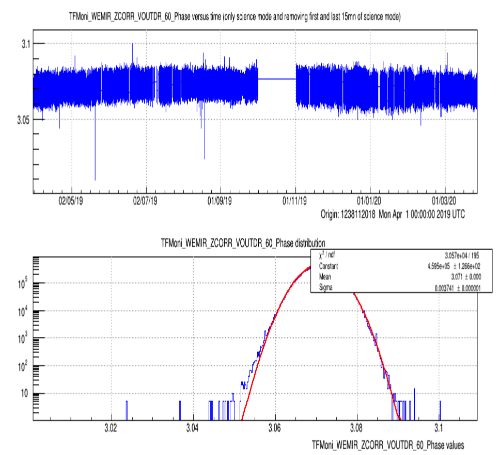

(d) phase WE, VOUT_DR , ∼60 Hz

Figure 29: TFMoni Phase near 60 Hz of the transfer function between WE coil voltages VOUT_UL, VOUT_UR, VOUT_DL and VOUT_DR and the longitudinal control loop signals Sc_WE_MIR_Z_CORR. For each plot, time evolution and fitted distribution are shown. By mistake in TFMoni configuration, for BS and PR, the online TF was not computed at the frequency of the injected line. Thus, the uncertainty on modulus and phase may differ from the one that would have been measured at the line frequency. Moreover, during O3b, the control signals were reduced, low enough so that the coils current monitoring was close to the sensing noise. As a consequence, the coherence between the two signals involved in the TF was reduced, hence the statistical fluctuations of the TF increased.

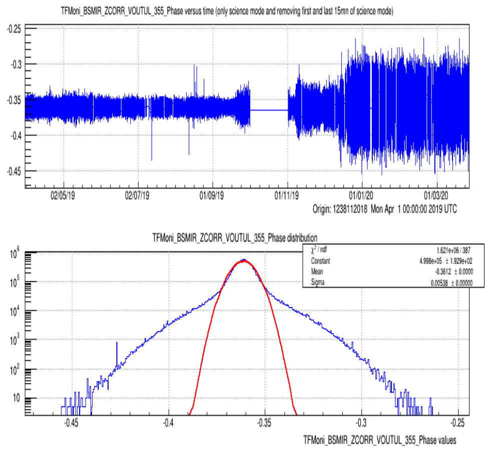

(a) phase BS, VOUT_UL , ∼355 Hz

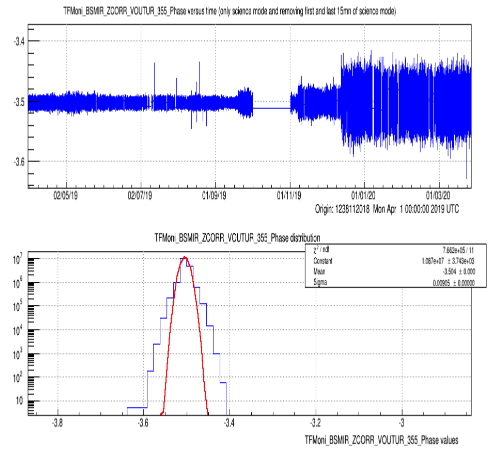

(b) phase BS, VOUT_UR , ∼355 Hz

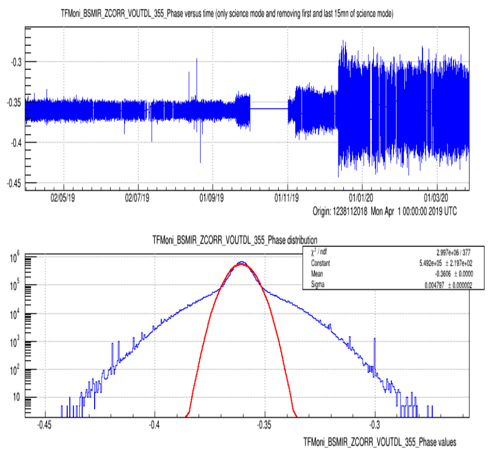

(c) phase BS, VOUT_DL , ∼355 Hz

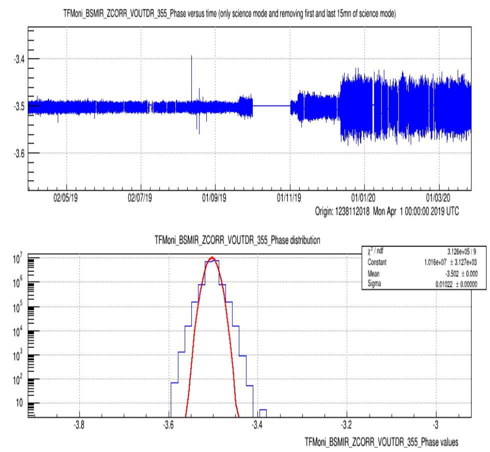

(d) phase BS, VOUT_DR , ∼355 Hz

Figure 30: TFMoni Phase near 355 Hz of the transfer function between BS coil voltages VOUT_UL, VOUT_UR, VOUT_DL and VOUT_DR and the longitudinal control loop signals Sc_BS_MIR_Z_CORR. For each plot, time evolution and fitted distribution are shown. By mistake in TFMoni configuration, for BS and PR, the online TF was not computed at the frequency of the injected line. Thus, the uncertainty on modulus and phase may differ from the one that would have been measured at the line frequency. Moreover, during O3b, the control signals were reduced, low enough so that the coils current monitoring was close to the sensing noise. As a consequence, the coherence between the two signals involved in the TF was reduced, hence the statistical fluctuations of the TF increased.

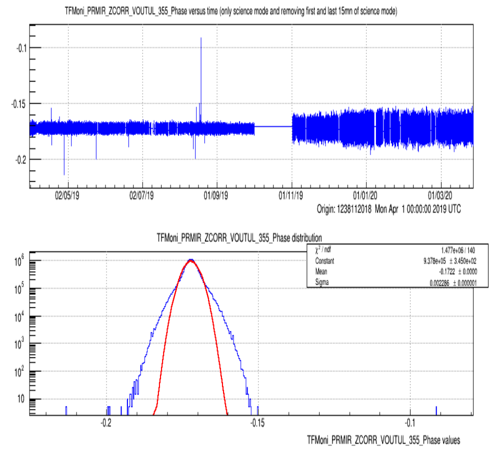

(a) phase PR, VOUT_UL , ∼355 Hz

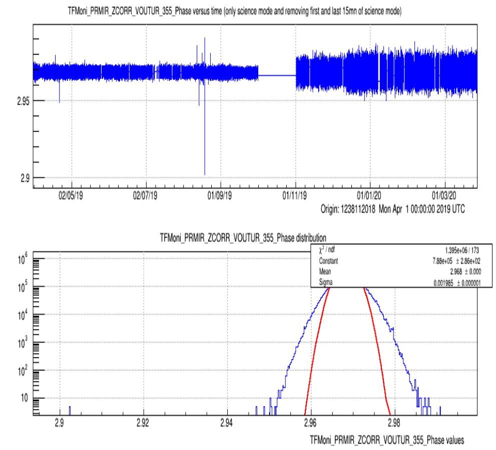

(b) phase PR, VOUT_UR , ∼355 Hz

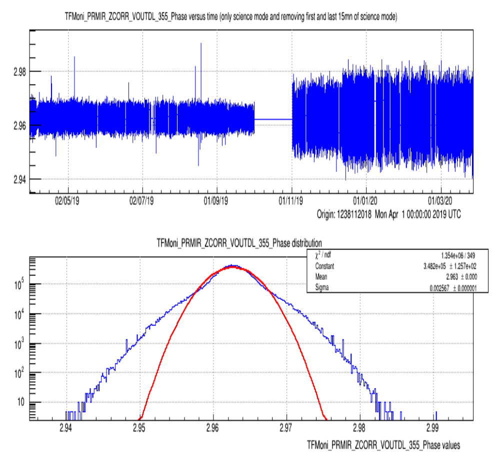

(c) phase PR, VOUT_DL , ∼355 Hz

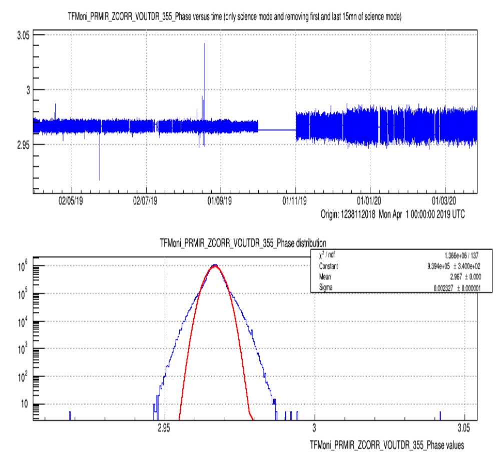

(d) phase PR, VOUT_DR , ∼355 Hz

Figure 31: TFMoni Phase near 355 Hz of the transfer function between PR coil voltages VOUT_UL, VOUT_UR, VOUT_DL and VOUT_DR and the longitudinal control loop signals Sc_PR_MIR_Z_CORR. For each plot, time evolution and fitted distribution are shown.

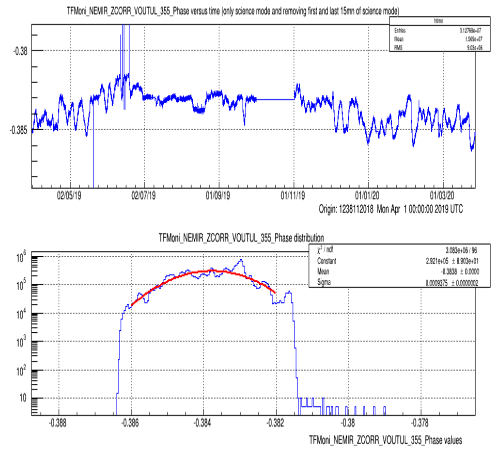

(a) phase NE, VOUT_UL , ~355 Hz

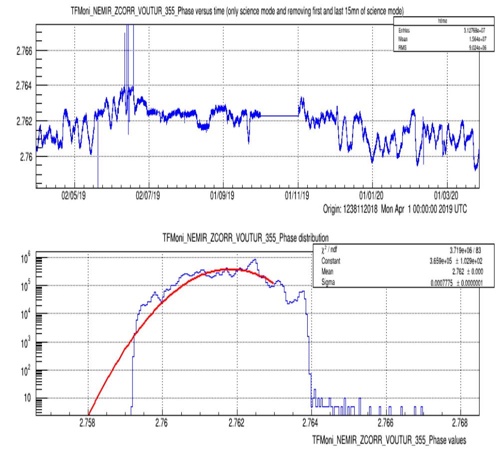

(b) phase NE, VOUT_UR , ~355 Hz

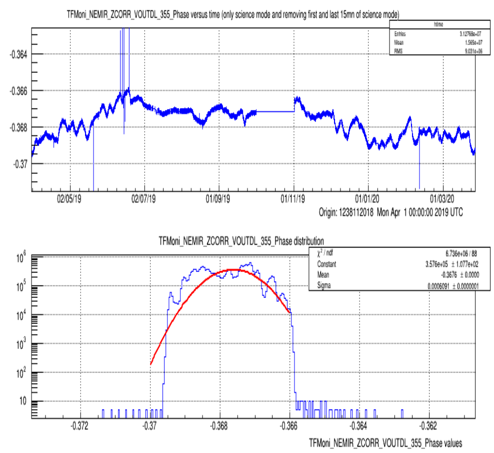

(c) phase NE, VOUT_DL , ~355 Hz

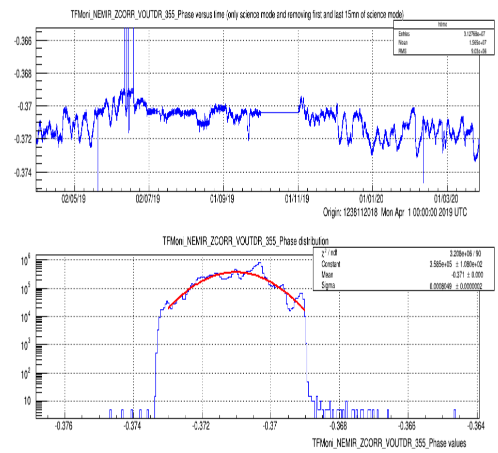

(d) phase NE, VOUT_DR , ~355 Hz

Figure 32: TFMoni Phase near 355 Hz of the transfer function between NE coil voltages VOUT_UL, VOUT_UR, VOUT_DL and VOUT_DR and the longitudinal control loop signals Sc_NE_MIR_Z_CORR. For each plot, time evolution and fitted distribution are shown. Around 355 Hz, the phase fluctuations, even small, are not gaussian and show various trends over days or weeks, in a similar way as what is observed for the modulus.

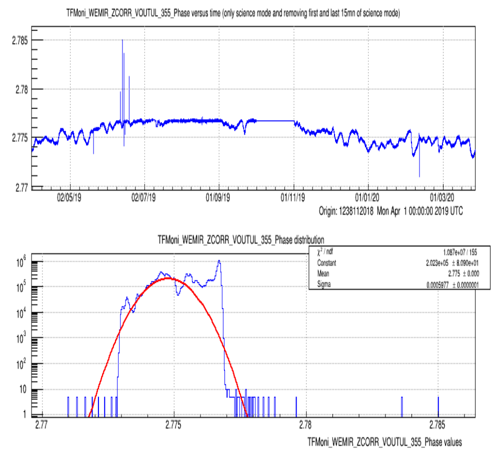

(a) phase WE, VOUT_UL , ∼355 Hz

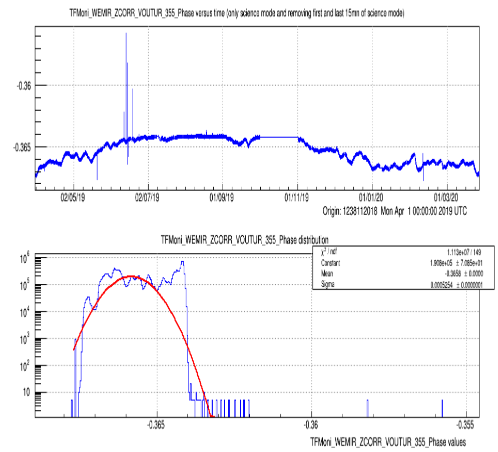

(b) phase WE, VOUT_UR , ∼355 Hz

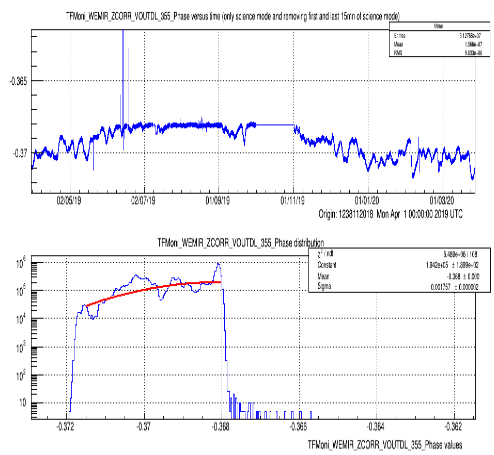

(c) phase WE, VOUT_DL , ∼355 Hz

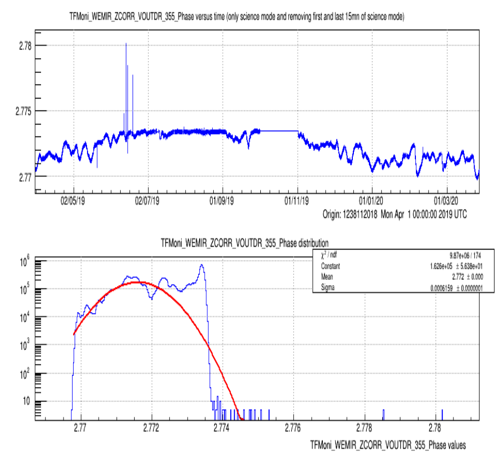

(d) phase WE, VOUT_DR , ∼355 Hz

Figure 33: TFMoni Phase near 355 Hz of the transfer function between WE coil voltages VOUT_UL, VOUT_UR, VOUT_DL and VOUT_DR and the longitudinal control loop signals Sc_WE_MIR_Z_CORR. For each plot, time evolution and fitted distribution are shown. Around 355 Hz, the phase fluctuations, even small, are not gaussian and show various trends over days or weeks, in a similar way as what is observed for the NE phase.

A TFMoni configuration used during O3

```
# Server /virgoApp/TFMoni/v1r0p1/Linux-x86_64-CL7/TFMoni.exe

CFG_PRIO 19                      # Main priority; 0 means no change (nice(0))
CFG_SCHEDAFFINITY 13-31
CFG_NOFILESAVE
CFG_PWD /virgoLog/VirgoOnline      # Current logfile path <path>/<cmName>

## Fd IN and OUT

FDIN_FRAME_MERGER 40 "/dev/shm/VirgoOnline/FbmAlp /dev/shm/VirgoOnline/HRec "
FDIN_TAG "V1:META_ITF_LOCK* V1:Sc_* V1:CAL* V1:PCAL* V1:Hrec_* V1:LSC_DARM"

FDOUT_ADD_PREFIX        "V1:" "*"
FDOUT_COMPRESSION  -1  0
FDOUT_STAT

FDOUT_FILE      /dev/shm/VirgoOnline/TFMoniToSt/V1-TFMoni 1  "V1:TFMoni_* "
FDOUT_FILE_CHECKSUM 0
FDOUT_CLEAN_DIR /dev/shm/VirgoOnline/TFMoniToSt 1 0 0.0 60

FDOUT_FILE      /dev/shm/VirgoOnline/TFMoni/V1-TFMoni 1  "V1:TFMoni_* V1:PCAL_*_PD*_power #SER V1:META_ITF_LOCK"
FDOUT_FILE_CHECKSUM 0
FDOUT_CLEAN_DIR /dev/shm/VirgoOnline/TFMoni 1 0 0.0 60


## Transfer Functions and Ratios

#  keyword  fftduration (sec)   maxaverage
CALI_TF_FFT_DEFAULT   10  12
# keyword  coherence min threshold
CALI_TF_COHEMIN       0.01


# keyword   chname1   chname2   freq (Hz)   fftduration (sec)   maxaverage   gain  delay (ms)  outname (optional)
# gain = the value multiplied to the result of the TF modulus
# delay = the time delay to be added (phase which will be subtracted to the TF phase is 2*pi*freq*delay)
# The results are TFMoni_outname_Modulus , TFMoni_outname_Phase and TFMoni_outname_Cohe
# computed at the frequency freq from the TF chname2/chname1

# NE Mirror
CALI_TF_ADD   NEMIR_ZCORR_VOUTDL_60   V1:Sc_NE_MIR_Z_CORR     V1:Sc_NE_MIR_VOUT_DL      62.5    0  0  0  0
CALI_TF_ADD   NEMIR_ZCORR_VOUTUL_60   V1:Sc_NE_MIR_Z_CORR     V1:Sc_NE_MIR_VOUT_UL      62.5    0  0  0  0
CALI_TF_ADD   NEMIR_ZCORR_VOUTDR_60   V1:Sc_NE_MIR_Z_CORR     V1:Sc_NE_MIR_VOUT_DR      62.5    0  0  0  0
CALI_TF_ADD   NEMIR_ZCORR_VOUTUR_60   V1:Sc_NE_MIR_Z_CORR     V1:Sc_NE_MIR_VOUT_UR      62.5    0  0  0  0
CALI_TF_ADD   NEMIR_ZCORRLN_ZCORR_60  V1:Sc_NE_MIR_Z_CORR     V1:Sc_NE_MIR_Z_CORR_LN    62.5    0  0  0  0

CALI_TF_ADD   NEMIR_ZCORR_VOUTDL_355  V1:Sc_NE_MIR_Z_CORR     V1:Sc_NE_MIR_VOUT_DL      357.5   0  0  0  0
CALI_TF_ADD   NEMIR_ZCORR_VOUTUL_355  V1:Sc_NE_MIR_Z_CORR     V1:Sc_NE_MIR_VOUT_UL      357.5   0  0  0  0
CALI_TF_ADD   NEMIR_ZCORR_VOUTDR_355  V1:Sc_NE_MIR_Z_CORR     V1:Sc_NE_MIR_VOUT_DR      357.5   0  0  0  0
CALI_TF_ADD   NEMIR_ZCORR_VOUTUR_355  V1:Sc_NE_MIR_Z_CORR     V1:Sc_NE_MIR_VOUT_UR      357.5   0  0  0  0
CALI_TF_ADD   NEMIR_ZCORRLN_ZCORR_355 V1:Sc_NE_MIR_Z_CORR     V1:Sc_NE_MIR_Z_CORR_LN    357.5   0  0  0  0

# WE Mirror
CALI_TF_ADD   WEMIR_ZCORR_VOUTDL_60   V1:Sc_WE_MIR_Z_CORR     V1:Sc_WE_MIR_VOUT_DL      61.5    0  0  0  0
CALI_TF_ADD   WEMIR_ZCORR_VOUTUL_60   V1:Sc_WE_MIR_Z_CORR     V1:Sc_WE_MIR_VOUT_UL      61.5    0  0  0  0
CALI_TF_ADD   WEMIR_ZCORR_VOUTDR_60   V1:Sc_WE_MIR_Z_CORR     V1:Sc_WE_MIR_VOUT_DR      61.5    0  0  0  0
CALI_TF_ADD   WEMIR_ZCORR_VOUTUR_60   V1:Sc_WE_MIR_Z_CORR     V1:Sc_WE_MIR_VOUT_UR      61.5    0  0  0  0
CALI_TF_ADD   WEMIR_ZCORRLN_ZCORR_60  V1:Sc_WE_MIR_Z_CORR     V1:Sc_WE_MIR_Z_CORR_LN    61.5    0  0  0  0

CALI_TF_ADD   WEMIR_ZCORR_VOUTDL_355  V1:Sc_WE_MIR_Z_CORR     V1:Sc_WE_MIR_VOUT_DL      356.5   0  0  0  0
CALI_TF_ADD   WEMIR_ZCORR_VOUTUL_355  V1:Sc_WE_MIR_Z_CORR     V1:Sc_WE_MIR_VOUT_UL      356.5   0  0  0  0
CALI_TF_ADD   WEMIR_ZCORR_VOUTDR_355  V1:Sc_WE_MIR_Z_CORR     V1:Sc_WE_MIR_VOUT_DR      356.5   0  0  0  0
CALI_TF_ADD   WEMIR_ZCORR_VOUTUR_355  V1:Sc_WE_MIR_Z_CORR     V1:Sc_WE_MIR_VOUT_UR      356.5   0  0  0  0
CALI_TF_ADD   WEMIR_ZCORRLN_ZCORR_355 V1:Sc_WE_MIR_Z_CORR     V1:Sc_WE_MIR_Z_CORR_LN    356.5   0  0  0  0

# BS Mirror
CALI_TF_ADD   BSMIR_ZCORR_VOUTDL_60   V1:Sc_BS_MIR_Z_CORR     V1:Sc_BS_MIR_VOUT_DL      62.8    0  0  0  0
CALI_TF_ADD   BSMIR_ZCORR_VOUTUL_60   V1:Sc_BS_MIR_Z_CORR     V1:Sc_BS_MIR_VOUT_UL      62.8    0  0  0  0
CALI_TF_ADD   BSMIR_ZCORR_VOUTDR_60   V1:Sc_BS_MIR_Z_CORR     V1:Sc_BS_MIR_VOUT_DR      62.8    0  0  0  0
CALI_TF_ADD   BSMIR_ZCORR_VOUTUR_60   V1:Sc_BS_MIR_Z_CORR     V1:Sc_BS_MIR_VOUT_UR      62.8    0  0  0  0
CALI_TF_ADD   BSMIR_ZCORRLN_ZCORR_60  V1:Sc_BS_MIR_Z_CORR     V1:Sc_BS_MIR_Z_CORR_LN    62.8    0  0  0  0

CALI_TF_ADD   BSMIR_ZCORR_VOUTDL_355  V1:Sc_BS_MIR_Z_CORR     V1:Sc_BS_MIR_VOUT_DL      357.8   0  0  0  0
CALI_TF_ADD   BSMIR_ZCORR_VOUTUL_355  V1:Sc_BS_MIR_Z_CORR     V1:Sc_BS_MIR_VOUT_UL      357.8   0  0  0  0
CALI_TF_ADD   BSMIR_ZCORR_VOUTDR_355  V1:Sc_BS_MIR_Z_CORR     V1:Sc_BS_MIR_VOUT_DR      357.8   0  0  0  0
CALI_TF_ADD   BSMIR_ZCORR_VOUTUR_355  V1:Sc_BS_MIR_Z_CORR     V1:Sc_BS_MIR_VOUT_UR      357.8   0  0  0  0
CALI_TF_ADD   BSMIR_ZCORRLN_ZCORR_355 V1:Sc_BS_MIR_Z_CORR     V1:Sc_BS_MIR_Z_CORR_LN    357.8   0  0  0  0

# PR Mirror
CALI_TF_ADD   PRMIR_ZCORR_VOUTDL_60   V1:Sc_PR_MIR_Z_CORR     V1:Sc_PR_MIR_VOUT_DL      62.3    0  0  0  0
CALI_TF_ADD   PRMIR_ZCORR_VOUTUL_60   V1:Sc_PR_MIR_Z_CORR     V1:Sc_PR_MIR_VOUT_UL      62.3    0  0  0  0
```

```
CALI_TF_ADD   PRMIR_ZCORR_VOUTDR_60   V1:Sc_PR_MIR_Z_CORR     V1:Sc_PR_MIR_VOUT_DR      62.3    0  0  0  0
CALI_TF_ADD   PRMIR_ZCORR_VOUTUR_60   V1:Sc_PR_MIR_Z_CORR     V1:Sc_PR_MIR_VOUT_UR      62.3    0  0  0  0

CALI_TF_ADD   PRMIR_ZCORR_VOUTDL_355  V1:Sc_PR_MIR_Z_CORR     V1:Sc_PR_MIR_VOUT_DL      357.3   0  0  0  0
CALI_TF_ADD   PRMIR_ZCORR_VOUTUL_355  V1:Sc_PR_MIR_Z_CORR     V1:Sc_PR_MIR_VOUT_UL      357.3   0  0  0  0
CALI_TF_ADD   PRMIR_ZCORR_VOUTDR_355  V1:Sc_PR_MIR_Z_CORR     V1:Sc_PR_MIR_VOUT_DR      357.3   0  0  0  0
CALI_TF_ADD   PRMIR_ZCORR_VOUTUR_355  V1:Sc_PR_MIR_Z_CORR     V1:Sc_PR_MIR_VOUT_UR      357.3   0  0  0  0

# CAL to Sc
CALI_TF_ADD   NEMIR_CALtoSc_2012      V1:CAL_NE_MIR_Z_CORR    V1:Sc_NE_MIR_Z_CORR    2012.5     0  0  0  0
CALI_TF_ADD   WEMIR_CALtoSc_2012      V1:CAL_WE_MIR_Z_CORR    V1:Sc_WE_MIR_Z_CORR    2012.5     0  0  0  0
CALI_TF_ADD   NIMIR_CALtoSc_2012      V1:CAL_NI_MIR_Z_CORR    V1:Sc_NI_MIR_Z_CORR    2012.5     0  0  0  0
CALI_TF_ADD   WIMIR_CALtoSc_2012      V1:CAL_WI_MIR_Z_CORR    V1:Sc_WI_MIR_Z_CORR    2012.5     0  0  0  0
CALI_TF_ADD   BSMIR_CALtoSc_2012      V1:CAL_BS_MIR_Z_CORR    V1:Sc_BS_MIR_Z_CORR    2012.5     0  0  0  0
CALI_TF_ADD   PRMIR_CALtoSc_2012      V1:CAL_PR_MIR_Z_CORR    V1:Sc_PR_MIR_Z_CORR    2012.5     0  0  0  0
CALI_TF_ADD   NEMAR_CALtoSc_2012      V1:CAL_NE_MAR_Z_CORR    V1:Sc_NE_MAR_Z_CORR    2012.5     0  0  0  0
CALI_TF_ADD   WEMAR_CALtoSc_2012      V1:CAL_WE_MAR_Z_CORR    V1:Sc_WE_MAR_Z_CORR    2012.5     0  0  0  0
CALI_TF_ADD   BSMAR_CALtoSc_2012      V1:CAL_BS_MAR_Z_CORR    V1:Sc_BS_MAR_Z_CORR    2012.5     0  0  0  0

# PCAL
CALI_TF_ADD   NEPCAL_PD1_PD2_30    V1:PCAL_NEB_PD1_power    V1:PCAL_NEB_PD2_power    34.5  0  0  0  0
CALI_TF_ADD   NEPCAL_PD1_PD2_60    V1:PCAL_NEB_PD1_power    V1:PCAL_NEB_PD2_power    63.5  0  0  0  0
CALI_TF_ADD   NEPCAL_PD1_PD2_355   V1:PCAL_NEB_PD1_power    V1:PCAL_NEB_PD2_power   359.0  0  0  0  0
CALI_TF_ADD   WEPCAL_PD1_PD2_30    V1:PCAL_WEB_PD1_power    V1:PCAL_WEB_PD2_power    36.5  0  0  0  0
CALI_TF_ADD   WEPCAL_PD1_PD2_60    V1:PCAL_WEB_PD1_power    V1:PCAL_WEB_PD2_power    60.5  0  0  0  0
CALI_TF_ADD   WEPCAL_PD1_PD2_355   V1:PCAL_WEB_PD1_power    V1:PCAL_WEB_PD2_power   355.5  0  0  0  0

# Compare DARM and CAL
CALI_TF_ADD   NEMIR_DARM_CAL_60     V1:CAL_NE_MIR_Z_CORR   V1:LSC_DARM      62.5  0  0  0  0
CALI_TF_ADD   NEMIR_DARM_CAL_355    V1:CAL_NE_MIR_Z_CORR   V1:LSC_DARM     357.5  0  0  0  0
CALI_TF_ADD   WEMIR_DARM_CAL_60     V1:CAL_WE_MIR_Z_CORR   V1:LSC_DARM      61.5  0  0  0  0
CALI_TF_ADD   WEMIR_DARM_CAL_355    V1:CAL_WE_MIR_Z_CORR   V1:LSC_DARM     356.5  0  0  0  0

# Compare DARM and PCAL
CALI_TF_ADD   NEMIR_DARM_PCAL_35      V1:PCAL_NEB_PD1_power   V1:LSC_DARM     34.5  0  0  0  0
CALI_TF_ADD   NEMIR_DARM_PCAL_60      V1:PCAL_NEB_PD1_power   V1:LSC_DARM     63.5  0  0  0  0
CALI_TF_ADD   WEMIR_DARM_PCAL_35      V1:PCAL_WEB_PD1_power   V1:LSC_DARM     36.5  0  0  0  0
CALI_TF_ADD   WEMIR_DARM_PCAL_60      V1:PCAL_WEB_PD1_power   V1:LSC_DARM     60.5  0  0  0  0


# Compare Hrec and NE PCAL
CALI_TF_ADD   NEMIR_HREC_HPCAL_35     V1:PCAL_NEB_PD1_hpcal   V1:Hrec_hoft_raw_20000Hz   34.5  0  24  0  0.122
# 112 from pcal +10 from end response               previous 0.148+10
CALI_TF_ADD   NEMIR_HREC_HPCAL_60     V1:PCAL_NEB_PD1_hpcal   V1:Hrec_hoft_raw_20000Hz   63.5  0  24  0  0.122
CALI_TF_ADD   NEMIR_HREC_HPCAL2_35    V1:PCAL_NEB_PD2_hpcal   V1:Hrec_hoft_raw_20000Hz   34.5  0  24  0  0.122
CALI_TF_ADD   NEMIR_HREC_HPCAL2_60    V1:PCAL_NEB_PD2_hpcal   V1:Hrec_hoft_raw_20000Hz   63.5  0  24  0  0.122

# Compare Hrec and WE PCAL
CALI_TF_ADD   WEMIR_HREC_HPCAL_35     V1:PCAL_WEB_PD1_hpcal   V1:Hrec_hoft_raw_20000Hz   36.5  0  24  0  0.122
CALI_TF_ADD   WEMIR_HREC_HPCAL_60     V1:PCAL_WEB_PD1_hpcal   V1:Hrec_hoft_raw_20000Hz   60.5  0  24  0  0.122
CALI_TF_ADD   WEMIR_HREC_HPCAL2_35    V1:PCAL_WEB_PD2_hpcal   V1:Hrec_hoft_raw_20000Hz   36.5  0  24  0  0.122
CALI_TF_ADD   WEMIR_HREC_HPCAL2_60    V1:PCAL_WEB_PD2_hpcal   V1:Hrec_hoft_raw_20000Hz   60.5  0  24  0  0.122

# Compare Hrec and NE CAL_NOISE
CALI_TF_ADD   NEMIR_HREC_HINJ_35      V1:CAL_NE_MIR_Z_NOISE   V1:Hrec_hoft_raw_20000Hz   37.5  0  0  2.43e+13  -0.337
CALI_TF_ADD   NEMIR_HREC_HINJ_75      V1:CAL_NE_MIR_Z_NOISE   V1:Hrec_hoft_raw_20000Hz   77.5  0  0  1.05e+14  -0.325
CALI_TF_ADD   NEMIR_HREC_HINJ_105     V1:CAL_NE_MIR_Z_NOISE   V1:Hrec_hoft_raw_20000Hz  107.5  0  0  2.03e+14  -0.315
CALI_TF_ADD   NEMIR_HREC_HINJ_135     V1:CAL_NE_MIR_Z_NOISE   V1:Hrec_hoft_raw_20000Hz  137.5  0  0  3.35e+14  -0.308

# Compare Hrec and WE CAL_NOISE
CALI_TF_ADD   WEMIR_HREC_HINJ_55      V1:CAL_WE_MIR_Z_NOISE   V1:Hrec_hoft_raw_20000Hz   56.5  0  0  6.66e+13  -0.301
CALI_TF_ADD   WEMIR_HREC_HINJ_105     V1:CAL_WE_MIR_Z_NOISE   V1:Hrec_hoft_raw_20000Hz  106.5  0  0  2.38e+14  -0.294
CALI_TF_ADD   WEMIR_HREC_HINJ_205     V1:CAL_WE_MIR_Z_NOISE   V1:Hrec_hoft_raw_20000Hz  206.5  0  0  9.00e+14  -0.286
CALI_TF_ADD   WEMIR_HREC_HINJ_405     V1:CAL_WE_MIR_Z_NOISE   V1:Hrec_hoft_raw_20000Hz  406.5  0  0  3.50e+15  -0.282

# Compare PCAL and CAL
CALI_TF_RATIO DARMCALNE_DARMPCALNE_60   NEMIR_DARM_CAL_60    NEMIR_DARM_PCAL_60
CALI_TF_RATIO DARMCALWE_DARMPCALWE_60   WEMIR_DARM_CAL_60    WEMIR_DARM_PCAL_60

# Compare CAL_NE and CAL_WE
CALI_TF_RATIO DARMCALNE60_DARMCALWE60    NEMIR_DARM_CAL_60    WEMIR_DARM_CAL_60
CALI_TF_RATIO DARMCALNE355_DARMCALWE355  NEMIR_DARM_CAL_355   WEMIR_DARM_CAL_355

# Compare PCAL_NE and PCAL_WE
CALI_TF_RATIO DARMPCALNE35_DARMPCALWE35    NEMIR_DARM_PCAL_35    WEMIR_DARM_PCAL_35
CALI_TF_RATIO DARMPCALNE60_DARMPCALWE60    NEMIR_DARM_PCAL_60    WEMIR_DARM_PCAL_60
```